

1 **Encoding time in neural dynamic regimes with distinct**
2 **computational tradeoffs**

3
4 Shanglin Zhou^{1,*}, Sotiris C. Masmanidis^{1,2}, Dean V. Buonomano^{1,3,*}

5
6
7
8
9
10
11
12
13
14
15
16
17
18 ¹Department of Neurobiology, University of California, Los Angeles, CA, USA.

19 ²California Nanosystems Institute, University of California, Los Angeles, CA, USA.

20 ³Department of Psychology, University of California, Los Angeles, CA, USA.

21 *Corresponding authors

22 Email: zhoushanglin@gmail.com (SZ), dbuono@ucla.edu (DVB)

23

24 **Abstract**

25 Converging evidence suggests the brain encodes time in dynamic patterns of neural
26 activity, including neural sequences, ramping activity, and complex dynamics. Most temporal
27 tasks, however, require more than just encoding time, and can have distinct computational
28 requirements including the need to exhibit temporal scaling, generalize to novel contexts, or
29 robustness to noise. It is not known how neural circuits can encode time and satisfy distinct
30 computational requirements, nor is it known whether similar patterns of neural activity at the
31 population level can exhibit dramatically different computational or generalization properties. To
32 begin to answer these questions, we trained RNNs on two timing tasks based on behavioral studies.
33 The tasks had different input structures but required producing identically timed output patterns.
34 Using a novel framework we quantified whether RNNs encoded two intervals using either of three
35 different timing strategies: scaling, absolute, or stimulus-specific dynamics. We found that similar
36 neural dynamic patterns at the level of single intervals, could exhibit fundamentally different
37 properties, including, generalization, the connectivity structure of the trained networks, and the
38 contribution of excitatory and inhibitory neurons. Critically, depending on the task structure RNNs
39 were better suited for generalization or robustness to noise. Further analysis revealed different
40 connection patterns underlying the different regimes. Our results predict that apparently similar
41 neural dynamic patterns at the population level (e.g., neural sequences) can exhibit fundamentally
42 different computational properties in regards to their ability to generalize to novel stimuli and their
43 robustness to noise—and that these differences are associated with differences in network
44 connectivity and distinct contributions of excitatory and inhibitory neurons. We also predict that
45 the task structure used in different experimental studies accounts for some of the experimentally
46 observed variability in how networks encode time.

47 **Author summary**

48 The ability to tell time and anticipate when external events will occur are among the most
49 fundamental computations the brain performs. Converging evidence suggests the brain encodes
50 time through changing patterns of neural activity. Different temporal tasks, however, have distinct
51 computational requirements, such as the need to flexibly scale temporal patterns or generalize to
52 novel inputs. To understand how networks can encode time and satisfy different computational
53 requirements we trained recurrent neural networks (RNNs) on two timing tasks that have
54 previously been used in behavioral studies. Both tasks required producing identically timed output
55 patterns. Using a novel framework to quantify how networks encode different intervals, we found
56 that similar patterns of neural activity—neural sequences—were associated with fundamentally
57 different underlying mechanisms, including the connectivity patterns of the RNNs. Critically,
58 depending on the task the RNNs were trained on, they were better suited for generalization or
59 robustness to noise. Our results predict that similar patterns of neural activity can be produced by
60 distinct RNN configurations, which in turn have fundamentally different computational tradeoffs.
61 Our results also predict that differences in task structure account for some of the experimentally
62 observed variability in how networks encode time.

63

64

65 **Introduction**

66 The ability to predict when external events will occur, and to detect temporal regularities
67 in the environment, are among the most fundamental computations the brain performs [1-5]. Thus,
68 the brain must have a rich repertoire of mechanisms to tell time and perform temporal
69 computations. Indeed, converging experimental and computational evidence indicates that a wide
70 range of different brain areas encode time through dynamically changing patterns of neural activity
71 [1, 6-10]. These patterns can take the form of monotonic ramping of the firing rates of neurons, or
72 so-called population clocks that can take the form of neural sequences or complex patterns of
73 neural activity [1, 11].

74 Experimental and computational analyses of the different neural encoding schemes for the
75 representation of time have focused primarily on the discrimination and production of isolated
76 intervals or durations. However, the computational requirements for processing temporal
77 information go far beyond merely requiring a timer to discriminate or produce a single duration or
78 interval. Some forms of temporal processing require the ability to smoothly scale a time-varying
79 motor pattern. For example, the ability to play a song on the piano at different tempos, or catch a
80 ball thrown at different speeds, requires that the underlying patterns of neural activity unfold at
81 different speeds [12-15]. Indeed, some tasks in animal studies explicitly require animals to exhibit
82 temporal scaling: depending on context cues or training blocks animals must temporally scale their
83 motor response [14, 16-18]. In contrast, other timing tasks are categorical in nature, for example
84 in the language domain phrasal boundaries are based in part on a categorical boundary of the pause
85 between phonemes—e.g., *great eyes x gray ties* [19, 20], similarly, in the motor domain, the
86 distinction between a double-click and two single clicks of a computer mouse is categorical.
87 Furthermore, in both the human and animal literature standard temporal bisection tasks require

88 subjects to make a two-alternative forced-choice categorical judgment regarding whether a
89 stimulus was short or long [21, 22].

90 It remains unclear if different computational requirements, such as the need to exhibit
91 temporal scaling or categorical timing, rely on similar or fundamentally different underlying neural
92 mechanisms to encode time. Consider a task in which an animal has to produce two intervals—
93 e.g., in response to two different sensory cues. Generally speaking, three encoding schemes could
94 allow the same network to produce these two different intervals: absolute timing, temporal scaling,
95 and stimulus-specific timing. Under *absolute* timing the neurons would respond at the same
96 moments in time during both the production of short and long intervals but additional neurons
97 would be active during the long interval; in a *temporal scaling* scheme neurons encode the same
98 relative time during both short and long intervals; and in a stimulus-specific code, there would be
99 unrelated patterns for each interval (e.g., entirely different neural sequences for the short and long
100 interval). These different schemes possess specific computational tradeoffs regarding their
101 suitability for temporal scaling versus categorical timing.

102 To date, a large diversity of neural signatures for the encoding of time—including scaling,
103 absolute timing, and stimulus-specific timing—have been observed during tasks that require
104 animals to discriminate or produce multiple intervals [14, 16-18, 23-30]. Here we propose that
105 some of this diversity is driven by task structure, and examine whether task structure influences
106 the way recurrent neural networks may encode time. To address this hypothesis we trained RNNs
107 on two tasks with identical output motor requirements and characterized how the networks encode
108 time and generalize to novel stimuli. Our results establish that subtle differences in task structure
109 lead to neural dynamic regimes that are better suited for temporal scaling or categorical timing.

110

111 **Results**

112 To begin to understand how task structure might shape how time is encoded in neural
 113 networks, we trained recurrent neural network models (RNNs) on one of two tasks inspired by
 114 previous experimental studies[14, 18, 23]. The RNNs were based on firing rate units with distinct
 115 populations of excitatory (80%) and inhibitory (20%) units. We will refer to the tasks as the 2-
 116 Context (Fig 1A) and 2-Stimulus (Fig 1B) tasks—critically, the timed motor outputs were identical

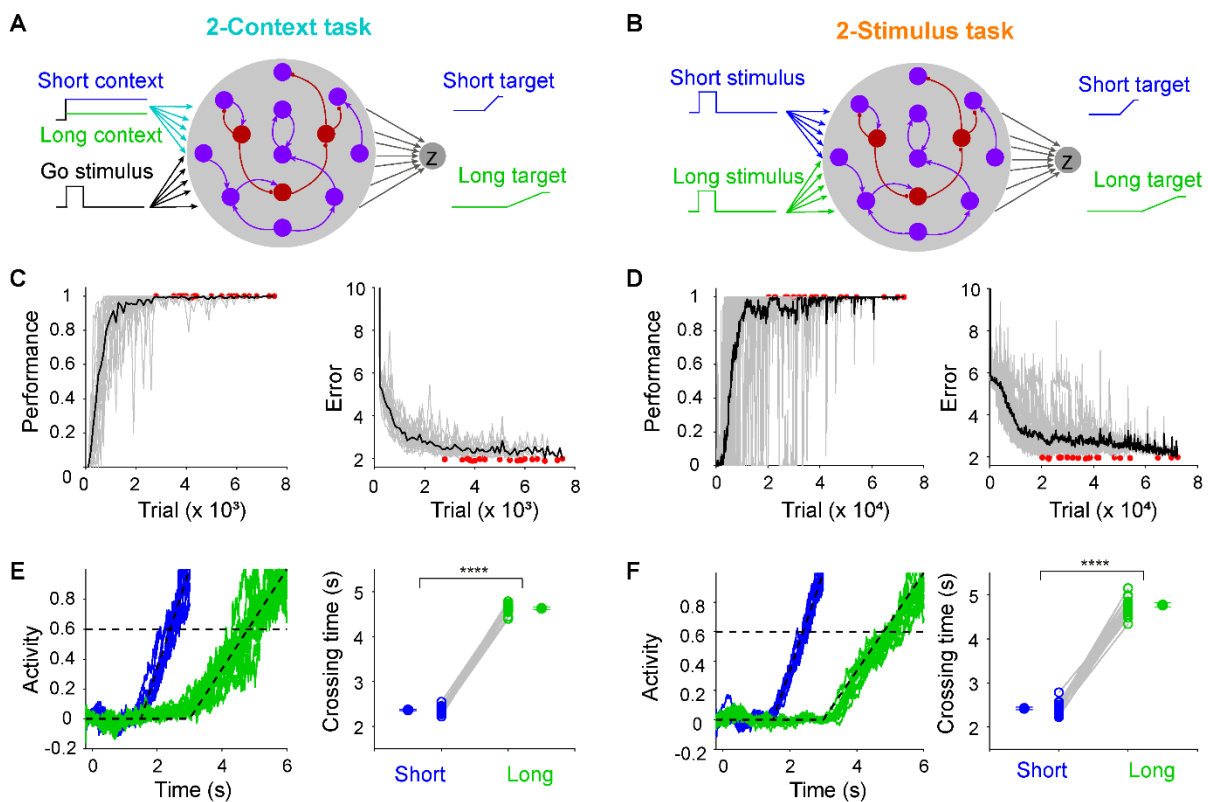


Fig 1. RNNs were trained on one of two timing tasks, both of which required producing the same timed output patterns. (A) Schematic of the 2-Context task. Each RNN was composed of 200 units—80% excitatory units (purple) and 20% inhibitory units (dark red)—and received a *go* and a *context* input. The context level signals the interval length to be produced: high = long (6 s, blue), low = short (3 s, green). (B) Schematic of the 2-Stimulus task. The same RNN was used in both tasks, except that the short- and long-interval was cued by two different inputs that were transiently activated. (C) Learning curve for the performance of 20 RNNs trained on the 2-Context task. Percentage of trials in which the timing of the output unit met criteria (left) and the error between the output and target (right). Gray traces represent results of each RNN, red dots denote the end of training for a given RNN, and the black trace represents the mean performance. (D) Same as in (C) but for the 2-Stimulus task. (E) Output traces across ten short (blue) and long (green) trials from an RNN trained on 2-Context task (left). Mean crossing times for long interval is significantly higher than that for short interval (right, $n = 20$ simulations, paired t test, $t_{19} = 77.70$, $P < 0.0001$). Dashed lines denote the targets and threshold. (F) Same as (E) but for 2-Stimulus task ($n = 20$ simulations, paired t test, $t_{19} = 45.79$, $P < 0.0001$).

118 in both tasks, requiring the production of either a short or long response. In the 2-Context task [e.g.,
119 14, 18], the *Go* cue (500 ms) indicated the onset of the trial ($t=0$), and the analog level of a
120 continuous context input signaled whether a trial is short or long. In the 2-Stimulus task, the short
121 and long interval trials were cued by two distinct transient inputs [23]. In both cases, the short and
122 long intervals consisted of a ramp-up of the output unit starting at the interval midpoint—a function
123 that approximates the behavioral response rate of animals trained to correctly time their
124 movements [23].

125 Performance was quantified by the ratio of correctly timed trials (see Methods) and the
126 error between the actual output and the target. RNNs trained on both tasks learned to produce the
127 same appropriately timed motor output (Fig 1C-F), although the RNNs trained on the 2-Context
128 task required fewer training trials to reach the same performance level ($n = 20$ simulations, two-
129 sample two-sided t-test, $t_{38} = 9.75$, $P < 0.0001$).

130

131 **Generalization to novel intervals**

132 Having shown that RNNs can produce the same temporal output patterns when trained on
133 two similar tasks, we next asked a key question: are there significant functional differences
134 between how the RNNs trained on the different tasks perform in response to novel input conditions?
135 To answer this question we examined generalization to untrained input conditions. To test the
136 generalization in the 2-Context task we varied the amplitude of the context cue between the range
137 of the trained values (0.75=short; 0.25=long). Interestingly the network exhibited fairly smooth
138 generalization—i.e., in response to intermediate context levels it produced intermediate motor
139 intervals (Fig 2A)—a finding consistent with previous computational studies [12, 14]. To test
140 generalization in the 2-Stimulus task we mixed the ratio of activation of the two stimulus cues—

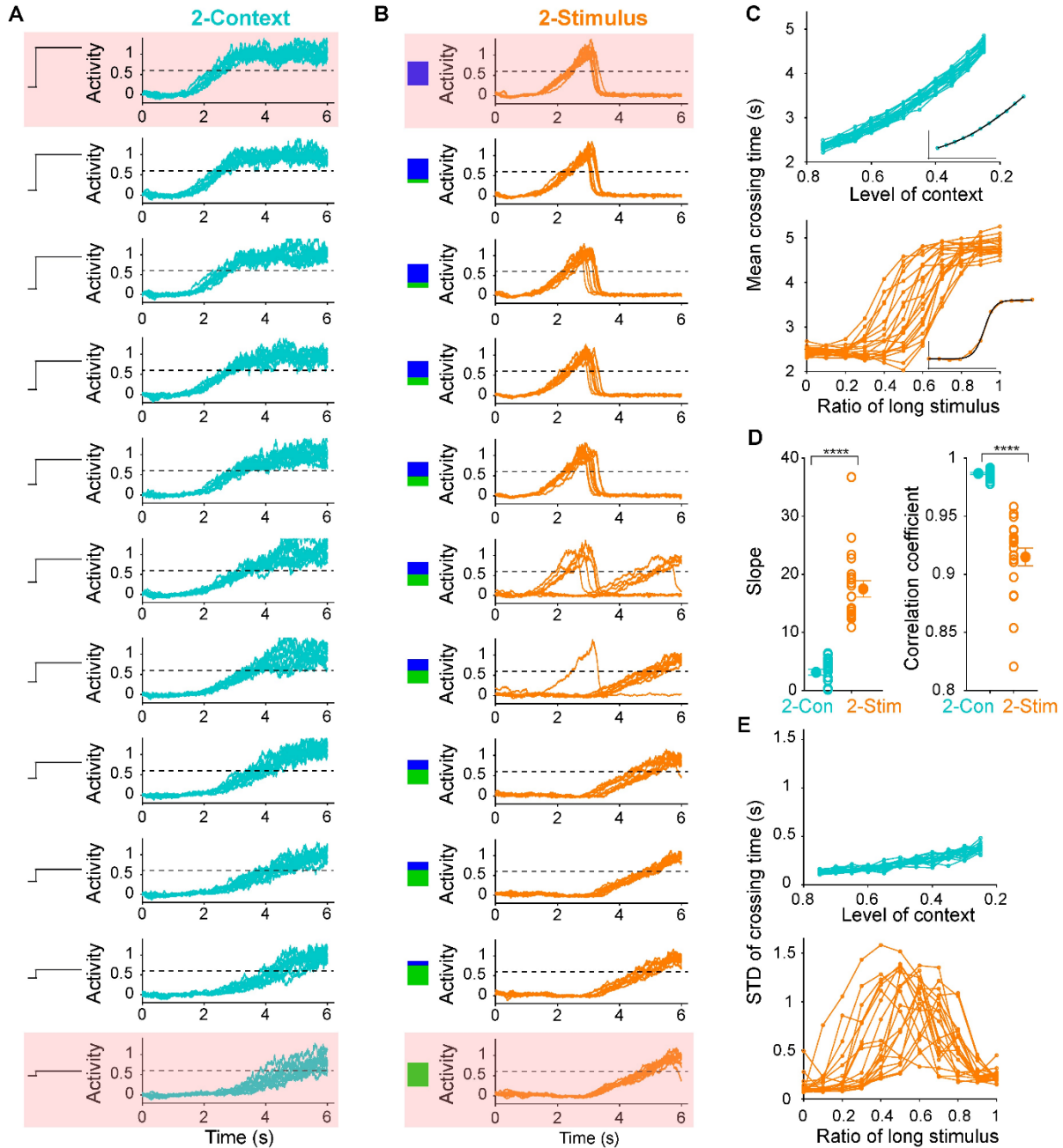


Fig 2. RNNs trained on the 2-Context task exhibited smooth generalization to novel intervals, while RNNs trained on the 2-Stimulus task exhibited categorical timing. (A) Output traces of an RNN trained on the 2-Context task across different context input levels. Dashed-black lines denote the output threshold used to quantify timing. Pink squares denote the trained conditions. (B) Similar to (A) but for the 2-Stimulus task. The blue and green squares represent the ratio of activation of the two input units. (C) Plots of the mean crossing time for each RNN across input conditions for the 2-Context (top) and 2-Stimulus (bottom) tasks. Insets, examples of the sigmoid-function fits for a single RNN (black). (D) Left, mean slope of the sigmoid fits for 2-Stimulus task is significantly higher than that for the 2-Context task ($n = 20$ simulations for each, two-sided t test, $t_{38} = 9.69$, $P < 0.0001$). Right, correlation coefficient between mean crossing times and input conditions for 2-Context task is significantly higher than that for the 2-Stimulus task ($n = 20$ simulations for each, two-sided t test on Fisher-transformed values, $t_{38} = 17.39$, $P < 0.0001$). The absolute correlation coefficient values are shown because in the 2-Context task the correlations are negative. (E) Standard deviations of the crossing times for each RNN in the 2-Context (top) and 2-Stimulus (bottom) tasks, as a function of input conditions.

142 during training [1, 0] corresponded to short and [0, 1] to long, during testing an intermediary 50/50
143 mixed input corresponded to [0.5 0.5]. In contrast to the 2-Context task, the RNNs trained on the
144 2-Stimulus task did not generalize, but the RNNs did not exhibit catastrophic degradation or
145 behave randomly. Rather, the RNNs expressed categorical timing: the output intervals clustered
146 near the short or long intervals (Fig 2B), essentially exhibiting a winner-take-all behavior.

147 To quantify these generalization patterns we measured the slope of a sigmoid fit between
148 input levels and output intervals, as well as the correlation between them (Fig 2C, D, see Methods).
149 The slope of the sigmoid was significantly less in the 2-Context fits—indicating a quasi-linear
150 relationship between context input level and produced intervals. The sigmoid slope was
151 significantly higher in the 2-Stimulus task, consistent with the prototypical sigmoidal signature of
152 categorical discrimination (Fig 2D, left panel). Similarly, the Pearson correlation coefficients
153 further supported the observation that the input-interval relationship was much more linear in the
154 2-Context task compared to the 2-Stimulus task (Fig 2D, right panel).

155 In addition to the above accuracy measures, we also quantified the precision of timing
156 across the different generalization conditions, as the standard deviation of the crossing time of
157 each trial (Fig 2E). The precision for the 2-Context task was high (low standard deviation) for all
158 the stimulus conditions. In contrast, in the middle range for the 2-Stimulus task precision was very
159 low. This was mainly due to categorical timing, i.e., in some stimulus conditions, the motor output
160 would randomly be attracted towards the short or long interval. Taken together, RNNs trained on
161 the 2-Context task were far superior at generalizing to novel intervals in terms of both timing
162 accuracy and precision, however, the RNNs trained on the 2-Stimulus task exhibited categorical
163 timing.

164 By design, the key difference in the tasks is that in the 2-Context task there is a continuous
165 input signaling the target interval throughout the task, whereas in the 2-Stimulus task two different
166 input weight vectors signal the desired interval, and each of these inputs is only active for a brief
167 period. To further determine whether the difference of the generalization patterns is robust to the
168 input parameters, we manipulated the ‘similarity of the inputs corresponding to the short and long
169 intervals in both tasks. Specifically, for the 2-Context task, different analog pairs of context level
170 were used, ranging from (0.95, 0.05) to (0.55,0.45). For the 2-Stimulus task, we gradually
171 increased the similarity by increasing the overlap ratio between the two inputs—proportions of the
172 same elements in the two input weights (S1 Fig **A**, **B**). In all five conditions, the generalization
173 performance for the 2-Context task was better than that for the 2-Stimulus task (S1 Fig **C**, **D**, and
174 **E**). While the tasks were designed to capture features of those used in behavioral experiments [14,
175 18, 23], in the 2-Context task the onset of the Go and Context stimuli redundantly signal trial onset
176 ($t=0$). Thus to understand the influence of the Go stimulus we also performed simulations without
177 the Go stimulus in the 2-Context task (S2 Fig **A**). As expected, omitting the Go stimulus left the
178 generalization performance largely unchanged compared to the standard 2-Context task with Go
179 stimulus, and still significantly better than that for the 2-Stimulus task (S2 Fig **B**). Finally, to
180 confirm that it is the presence of the continuous context input that plays a critical role in the
181 differential generalization patterns, we performed “2-Context” simulations in which the short and
182 long intervals were cued by a transient “context” stimulus rather than a persistent context input.
183 Consistent with our expectations based on previous results[12, 14, 30], in the absence of a
184 continuous context input the generalization was more consistent with categorical timing (S3 Fig)

185 Additional simulations confirmed that the difference of the generalization performance
186 between the 2-Context task and 2-Stimulus were robust to the change of several hyperparameters

187 including the initial gain (S4 Fig A-C) and connection probability (S5 Fig A-C) of the recurrent
188 weights.

189 **Potential dynamic regimes underlying the encoding of multiple** 190 **intervals**

191 Converging experimental and theoretical evidence indicates that a broad range of neural
192 dynamic regimes encode time. But to date, these different regimes have not been contrasted in
193 terms of their ability to encode multiple intervals and lead to generalization or categorical timing,
194 or robustness to noise. Here we examine three broad potential strategies for the encoding of two
195 intervals: scaling, absolute, and stimulus-specific codes. To illustrate these three strategies we
196 consider how a network of neurons could encode both a short (3 s) and long (6 s) intervals (Fig
197 3)—note that while we use neural sequences to contrast the three encoding schemes, the same
198 classification applies to other codes for time, including ramping activity. In a temporal scaling
199 strategy (Fig 3A), the dynamics of each unit for the short interval is linearly scaled in time to
200 produce the long interval (Fig 3B), which at the level of single units leads to two overlapping
201 curves (Fig 3C). Similarly, when the neural trajectories of the entire population are projected into
202 a low-dimensional space by principal component analysis the trajectories are also overlapping (Fig
203 3D). Under an absolute encoding strategy (Fig 3, middle panels) the temporal profile of each unit
204 during the short interval does not change during the long interval. The long interval simply relies
205 on recruiting additional neurons that have later temporal fields. Thus in PCA space, the curves for
206 the short interval matched the first half of that for the long interval. In a stimulus-specific strategy
207 (Fig 3, right panels), the temporal profile of each neuron is essentially uncorrelated during the
208 short and long intervals. Thus in PCA space, the trajectories of the neural patterns of activity
209 produced during the short and long intervals are distinct from one another.

210 Importantly, these encoding strategies are not necessarily mutually exclusive within a
 211 population of neurons. A network could use mixed encoding strategies in which different neurons

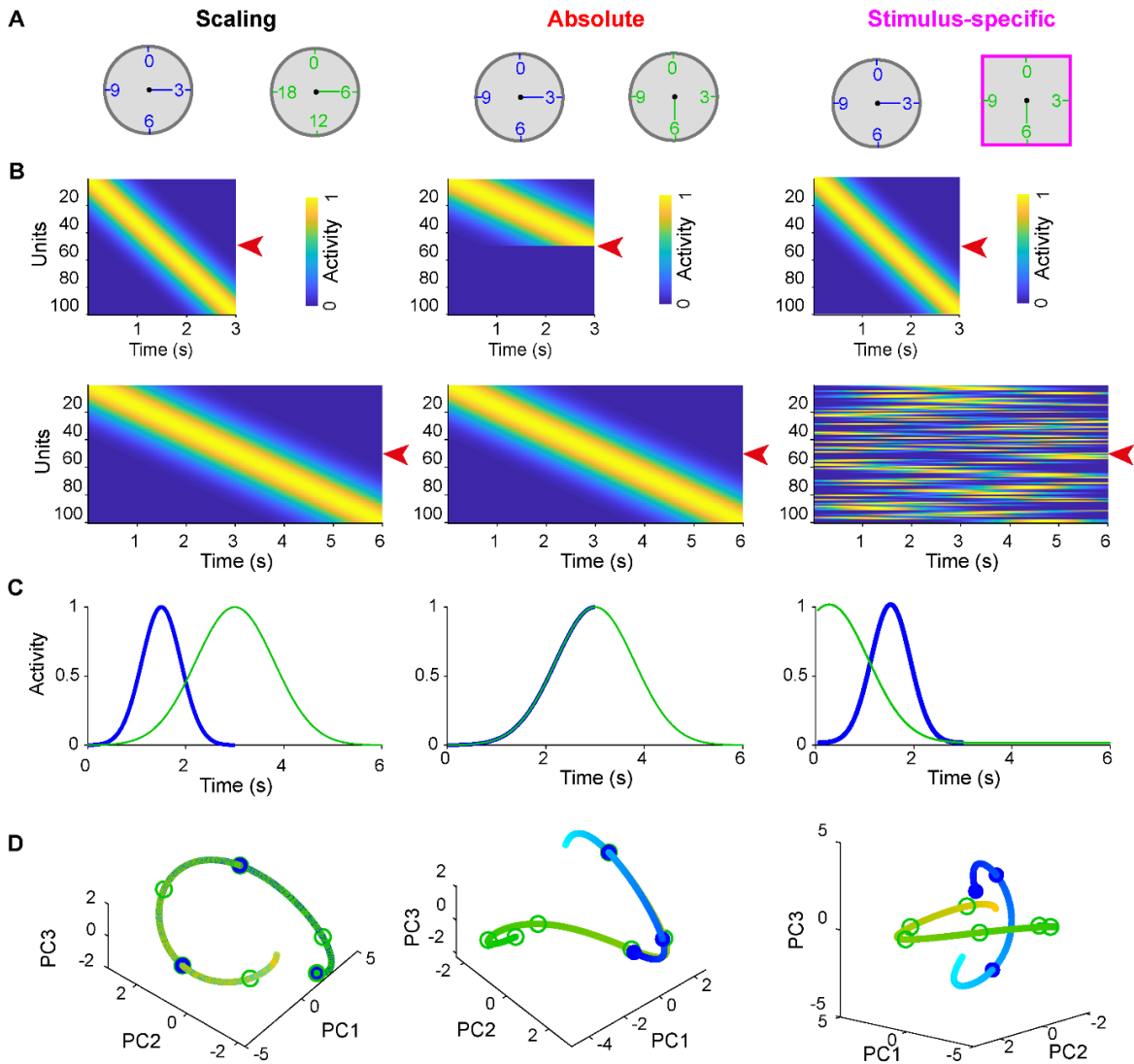


Fig 3. Three strategies for the encoding of two intervals by the same group of neurons. (A) Schematic of three potential strategies for timing two intervals: scaling, absolute, and stimulus-specific from left to right. (B) Prototypical dynamics for each of the encoding schemes for a population of units during production of the short (top) and long (bottom) intervals. (C) Activity traces of the units denoted by the red arrows in (B) for short (blue) and long (green) intervals. (D) Trajectories of three PCA components for short (cyan-blue) and long (yellow-green) interval for the corresponding population dynamics. The gradient colors (from the light to the dark) denote the flow of time. Circles denote the time points of the 1st, 2nd, 3rd, 4th, 5th, and 6th seconds.

212
 213 are best described as scaling from one interval to another, while others encode absolute time. It is
 214 also possible that the dynamics of a given unit exhibit an absolute code early in a trial followed by

215 scaling later in the trial. Note, however, that it would not make sense to consider a case in which
216 a unit undergoes scaling early in a trial and then exhibits absolute timing.

217 We next describe how to quantify these three schemes both at the level of the neural
218 population and of individual neurons in RNNs trained on either 2-Context or 2-Stimulus tasks.

219

220 **Task structure differentially shapes the time encoding strategies at** 221 **the population level**

222 In order to visualize the internal dynamics of the RNNs we first plotted the normalized
223 activity observed during the short and long intervals sorted according to the latency of peak activity
224 for each unit during the short interval (Fig 4A-B, left panels), and sorted by the long intervals (Fig
225 4A-B, right panels). Interestingly, although the target output was a ramping pattern, relatively few
226 RNN units appeared to be ramping. Rather, the global activity patterns in both tasks might be best
227 conceptualized as neural sequences. Yet, while the self-sorted sequences appeared to be visually
228 similar for both tasks, the cross-sorted sequences were dramatically different. Specifically, in the
229 2-Context task it appeared that neurons fired in the same order for both the short and long
230 intervals—suggestive of a scaling encoding strategy. However, in the 2-Stimulus task the cross-
231 sorted PSTHgrams revealed a more complex relationship between the spatio-temporal patterns of
232 activity during the short and long intervals—suggestive of a more stimulus-specific encoding
233 strategy.

234 To quantify if the neural dynamics observed in the 2-Context and 2-Stimulus tasks were
235 more consistent with a scaling, absolute, or stimulus-specific code, we first developed a stimulus-
236 specific index (SSI_{pop}) based on previously described geometric approaches [12, 30, 31]. We
237 started with the cross-Euclidean distance matrix between population dynamics for short and long

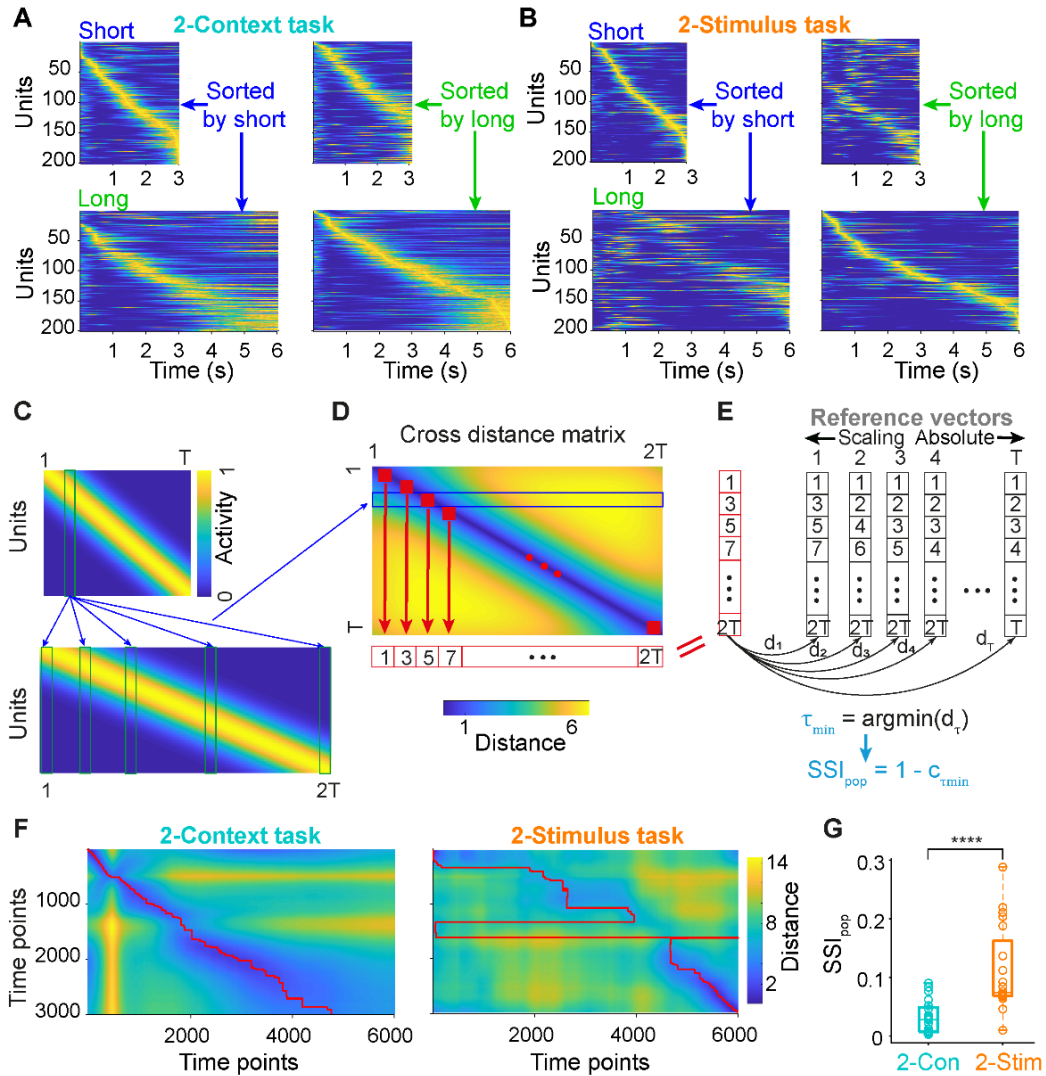


Fig 4. Distinct population dynamics in RNNs trained on the 2-Context and 2-Stimulus task. (A) Population activity for short (top) and long (bottom) intervals sorted according to the peak activity latency during short (left) and long (right) intervals for RNNs trained on the 2-Context task. (B) Same as A for the 2-Stimulus task. (C), (D), (E) Schematic of the calculation of the stimulus-specific index (SSI_{pop}). A prototypical neural sequence that undergoes pure temporal scaling from the short (top) to long (bottom) intervals is used as an example (C). The vectors of the pairwise time points from the short and long dynamics are used to calculate all pairwise Euclidean distances, and these pairwise distances comprise the cross-distance matrix (D), in which a row (e.g., blue rectangle) represents the distances between one column vector of short dynamics and all column vectors during the long dynamics. The minimal index vector (red vectors in (D) and (E)) represents the indices along the x-axis that corresponds to the minimum distances for each row of the cross-distance matrix (red squares). A series of reference vectors that vary from pure scaling to pure absolute timing (black vectors) are compared to the minimal index vector, and a value τ_{min} is defined as the τ at which the pairwise distance reaches the minimum. Finally, the correlation coefficient between the minimal index vector and the absolute-scaling reference vector at τ_{min} is used to calculate SSI_{pop} . (F) Cross distance matrices for an example simulation of the 2-Context (left) and 2-Stimulus tasks (right). Red lines denote the indices of the minimum values for each row. (G) SSI_{pop} for RNNs trained on the 2-Stimulus task is significantly higher than that for 2-Context task ($n = 20$ simulations for each, two-sided Wilcoxon rank-sum test $P < 0.0001$). Boxplot: central lines, median; bottom and top edges, lower and upper quartiles; bottom and top whiskers: extremes.

239 intervals (see Methods), which compares the similarity of the activity across all time pairs during
240 the short and long intervals (Fig 4C-D, example based on a case of perfect scaling of the entire
241 population). We then extracted the index (time bin of the long interval) corresponding to the
242 minimum value along each row of the cross-time distance matrix (red square in Fig 4D), which
243 results in a vector of the time points that in the long-interval that are closest to each of the time
244 points in the short-interval: the minimal index vector (red row vector in Fig 4D and column vector
245 in Fig 4E). This minimal index vector was then matched to all possible reference vectors
246 representing perfect scaling codes to a perfect absolute code (black column vectors in Fig 4E) by
247 computing the distances d_{τ} between each pair (Fig 4E). The reference vector with the minimum
248 distance ($d_{\tau_{\min}}$) to the minimal index vector denoted the best absolute-scaling vector. The
249 correlation ($c_{\tau_{\min}}$) between the best absolute-scaling vector and the minimal index vector
250 determines how good the match is: 1.0 reflects perfect scaling, absolute timing, or a perfect mixture
251 of absolute and scaling code. However, the correlation will be low or even negative in the case of
252 a stimulus-specific code. Therefore, SSI_{pop} was defined by $1 - c_{\tau_{\min}}$ (Fig 4E), meaning that both
253 perfect scaling and absolute timing would result in an $SSI_{\text{pop}}=0$, and the stimulus-specific code
254 would be proportional to SSI_{pop} .

255 We calculated SSI_{pop} for all 20 RNNs in both the 2-Context and 2-Stimulus tasks. SSI_{pop}
256 was significantly higher during the neural dynamics of the 2-Stimulus task compared to the 2-
257 Context task (Fig 4G), indicating that dynamics observed during the 2-Stimulus task reflected a
258 stimulus-specific encoding strategy more so than the 2-Context task. However, consistent with the
259 visual inspection of the dynamics and distance matrices (Fig 4A, F), it is clear that the 2-Stimulus
260 task was not entirely accounted for by a stimulus-specific strategy, suggesting a mixed code. Thus

261 we next examined the three encoding strategies from the perspective of the individual units in the
262 network.

263

264 **Task structure shapes timing encoding strategy at the level of single** 265 **units**

266 To understand whether the encoding of the short and long intervals was most consistent
267 with a scaling, absolute, or stimulus-specific code at the level of single units, we used a previously
268 described measure of absolute-versus-scaling index (ASI) [23], and incorporated a novel stimulus-
269 specific index (SSI_{unit}) into the framework. Much as SSI_{pop} quantifies how different the dynamics
270 of two neural populations are, SSI_{unit} quantifies how different the firing-rate profiles of a unit are
271 during a short versus long trial (see Methods). More specifically, for a given unit, a high SSI_{unit}
272 implies the temporal profiles during two trials are not related to each other through scaling,
273 absolute timing, or a mixture of both with the absolute part followed by the scaling part. A low
274 SSI_{unit} implies that the temporal profiles are related through scaling, absolute timing, or a mixture
275 of both, thus justifying the use of the ASI to further quantify scaling versus absolute timing. To
276 calculate the SSI_{unit} we first time-warped the temporal profile of a unit during the long interval into
277 a series of reference absolute-scaling traces spanning from pure scaling to pure absolute timing
278 with a mixture of both in between (Fig 5A). These reference traces were defined by a “breaking
279 point” τ marking the transition from absolute timing to scaling ($\tau=0$ reflects perfect scaling and τ
280 $=T_{\text{short}}$ reflect absolute timing). All reference traces were compared with the short dynamics by
281 computing the Euclidean distance at each τ (d_{τ}). The reference trace with the minimum distance
282 (d_{min}) denoted the best match with the actual temporal profile of the unit. Finally, as with SSI_{pop} ,
283 the SSI_{unit} was defined as 1.0 minus the correlation between the temporal profile during the short

284 intervals and the reference trace at τ_{\min} ($c_{\tau_{\min}}$). For a given unit with a low SSI_{unit} (≤ 0.5), we went
285 on to calculate its ASI which is also based on τ_{\min} (see Methods). With the SSI_{unit} and ASI in hand,
286 we classified a given unit as either a stimulus-specific unit ($SSI_{\text{unit}} > 0.5$), a scaling unit ($SSI_{\text{unit}} \leq 0.5$,
287 $ASI \leq 0.5$), or an absolute unit ($SSI \leq 0.5$, $ASI > 0.5$) (Fig 5B).

288 This approach allowed us to classify each unit of the network and contrast the distribution
289 of temporal classifications between the 2-Context and 2-Stimulus tasks. These analyses revealed
290 that RNNs exhibit a mixed encoding strategy, exhibiting a broad range of scaling, absolute, and
291 stimulus-specific units (Fig 5C). However, there were highly significant differences in the
292 distributions of temporal classes between the RNNs trained on the 2-Context and 2-Stimulus tasks
293 (Fig 5D). The 2-Context RNNs were dominated by scaling units, while 2-Stimulus RNNs had
294 more stimulus-specific units. The results partially explain why 2-Context RNNs were better at
295 generalizing to novel intervals. Because our RNN structure obeyed Dale's law it was possible to
296 contrast the encoding strategies of excitatory and inhibitory neurons. Interestingly the distribution
297 of scaling, absolute, and stimulus-specific cells appeared similar between excitatory and inhibitory
298 neurons (Fig 5D).

299 To establish a causal relationship between the distribution of temporal classes to the
300 functional properties of the RNNs we selectively deleted units of different classes from the RNNs
301 trained on both tasks (S6 Fig A). We then investigated how the performance changed in response
302 to these deletions. Performance and error across six deletion manipulations (stimulus-specific,
303 scaling, and absolute temporal-classes for the excitatory and inhibitory populations) revealed
304 inhibitory scaling units more severely impaired RNN function (S6 Fig B, C) for the 2-Context task.
305 In contrast, no single manipulation condition more severely affected both performance and error
306 in the 2-Stimulus task (S6 Fig D, E). Somewhat surprisingly these results reveal that in the case of

307 the 2-Context task a single subtype of inhibitory neurons—those that were classified as scaling
 308 units—are the most critical for network dynamics and encoding time. Whereas in the 2-stimulus
 309 task the coding strategy can be considered to be truly mixed, in the sense that all temporal classes
 310 and excitatory-inhibitory neurons seem to contribute more or less equally to the underlying
 311 dynamics and the encoding of time.

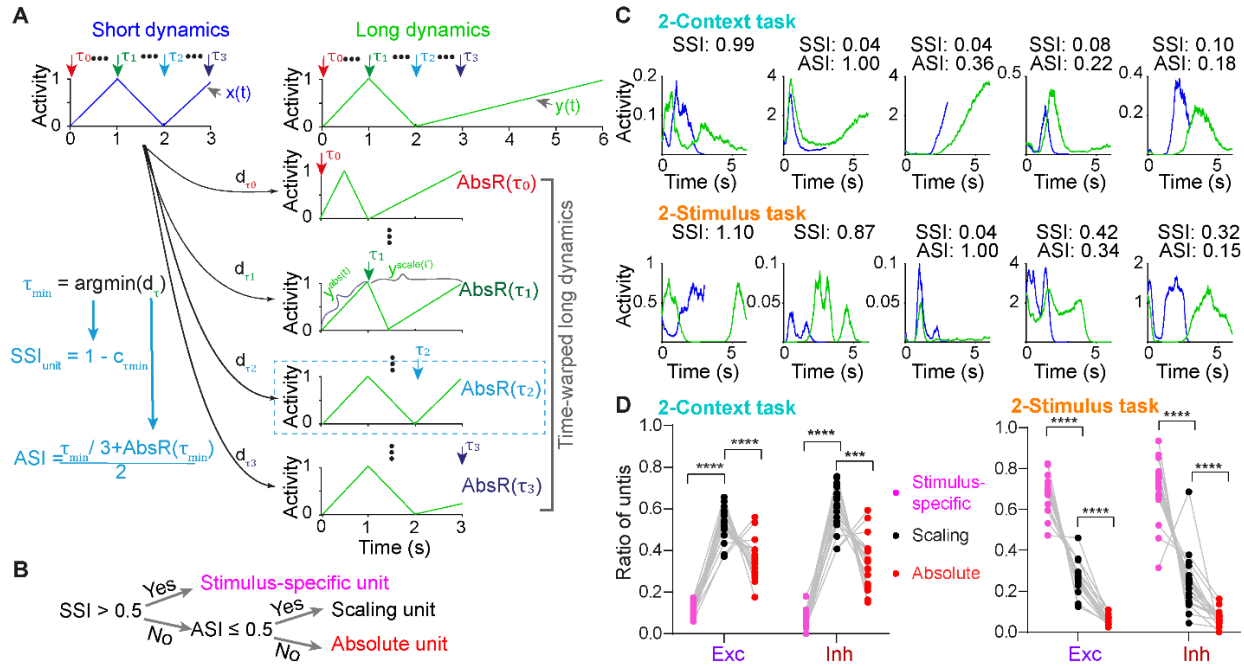


Fig 5. Different distribution of stimulus-specific, scaling, and absolute units between the 2-Context and 2-Stimulus tasks. (A) Schematic of the definitions of the stimulus-specific index (SSI_{unit}) and absolute vs. scaling index (ASI) at the single unit level. Consider a hypothetical firing rate profile of a unit during a short (blue, $x(t)$) and long (green, $y(t)$) trial. As described in Methods, a series of time-warped long dynamics are generated at breaking point τ_x : before τ_x the dynamics are the same during both the short and long intervals (absolute timing, $y^{abs}(t)$); after τ_x the dynamics is the scaled version of the corresponding original long dynamics ($> \tau_x$, scaling timing, $y^{scale}(t')$). Pairwise Euclidean distance between short dynamics and all time-warped long dynamics are computed at each τ_x . The point at which the distance is minimal defines τ_{min} and is used to compute the SSI_{unit} as in SSI_{pop} . To compute the ASI, a normalized measure of the distance before and after τ_{min} is calculated (AbsR) as in described in Methods to quantify the weighting factor for the absolute part (before τ_{min}) and the scaling part (after τ_{min}). ASI is defined by τ_{min} and the weighting factor based on AbsR(τ_{min}). (B) For a given unit, the SSI_{unit} is computed first, and if the SSI_{unit} is higher than 0.5, it is classified as stimulus-specific unit. If the SSI_{unit} is lower than 0.5, its ASI is computed, and it is classified as scaling unit if its ASI is lower than 0.5, otherwise as an absolute unit. (C) Dynamics of five example unit traces for short (blue) and long (green) intervals for the 2-Context (top) and 2-Stimulus (bottom) tasks, the corresponding SSI and ASI values are shown on top. Notice that for a given unit, ASI is only computed only when its SSI_{unit} is lower than 0.5. (D) For the 2-Context task (left), most units are classified as scaling units—for both excitatory and inhibitory units ($n = 20$ simulations, two-way ANOVA with repeated measures, for the unit classification factor: $F_{(2, 38)} = 114.4$ and $P < 0.0001$, posthoc Tukey tests $P < 0.0001$). For the 2-Stimulus task (right), stimulus-specific units are the most common ($n = 20$ simulations, two-way ANOVA with repeated measures, $F_{(2, 38)} = 181.5$ and $P < 0.0001$, posthoc Tukey tests $P < 0.0001$).

313 **Task structure differentially shapes the relationship between** 314 **recurrent dynamics and input/output space**

315 After quantifying how the different task structures shaped the encoding strategies, we
316 sought to determine if the differences can be understood in terms of the relationship between RNN
317 dynamics and the input/output subspaces. Generally, recurrent dynamics is driven by two sources:
318 the interaction between the inputs and input weights, and between recurrent activity and recurrent
319 weights. To start to understand how the inputs affected the recurrent dynamics and how the
320 recurrent dynamics would lead to the output through the output weights, we first performed the
321 principal component analysis on the concatenated dynamics of both intervals for each task (S7 Fig
322 **A, B**)—the first three PCs for the 2-Context task explained more variance than that for the 2-
323 Stimulus task ($88.15\pm 0.75\%$ vs $69.72\pm 0.73\%$, S7 Fig **C**). We then projected the recurrent
324 dynamics into the low dimensional space spanned by the first three PCs (S7 Fig **A, B**). Visually in
325 PC space, the dynamics of the two intervals for 2-Context task orbited close to each other, while
326 that for the 2-Stimulus task formed two distinct trajectories—consistent with our findings that 2-
327 Context task tended to use an absolute-scaling strategy while 2-Stimulus, a stimulus-specific
328 strategy. These observations were further established by plotting the dynamics in response to
329 generalization conditions (Fig 2). In the 2-Context task the dynamics across different inputs
330 smoothly transitioned to nearby trajectories, while in the 2-Stimulus task the trajectories clustered
331 around the two trained (short and long) trajectories (S8 Fig).

332 To directly compare the relationship between the recurrent dynamics across time and the
333 input/output weights, we projected the input weights—Input_{Go} and Input_{Context} for the 2-Context
334 task, Input_{Short} and Input_{Long} for the 2-Stimulus task—and the output weights into the same PC
335 space. We then computed the pairwise angles between the projected input/output vectors and each

336 segment vector of recurrent dynamics across time (see Methods) (S7 Fig A) for both tasks.
337 Interestingly, for the 2-Context task the dynamics of both intervals first evolved in the Input_{Go}
338 input direction as revealed by the small angle for the first 2 segments. After that, both trajectories
339 stayed in a plane almost orthogonal to the Go input till the end of the trial. The dynamics were
340 almost orthogonal to the $\text{Input}_{\text{Context}}$ at the beginning (with angles close to 90 degrees) and then the
341 angle decreased in the middle period and increased again to about 90 degrees at the later period.
342 Finally, for output weights, the angle stayed close to 90 degrees at the beginning then it decreased
343 to a low level till the end of the trial indicating that the dynamics followed the output weights
344 directions in the later period of the trials to better generate the target ramp starting at the middle
345 point of each trial (S7 Fig D).

346 For the 2-Stimulus task, the dynamics of short and long intervals started to follow their
347 corresponding input directions and then went to the opposite directions after input offset and stayed
348 almost orthogonal thereafter. While for the output weights, the angle started at around 90 degrees
349 and then decreased around the start point of the target ramp then it increased at the end of the trials
350 to the opposite direction (S7 Fig E).

351

352 **Task structure differentially shapes the learned recurrent synaptic** 353 **connectivity**

354 Ultimately the task-specific differences in RNN dynamics must be attributed to differences
355 in input structure and the recurrent weight matrix. Thus we next characterized the relationship
356 between the recurrent weight matrices and performance. Since our RNNs respected Dale's law,
357 we grouped weights into the four standard subtypes: all excitatory to excitatory unit connections
358 ($E \rightarrow E$), all excitatory to inhibitory unit connections ($E \rightarrow I$), all inhibitory to excitatory unit

359 connection (I→E), and all inhibitory to inhibitory unit connections (I→I). We then completely
 360 deleted each group of synapses and quantified the change in output performance (Fig 6A).

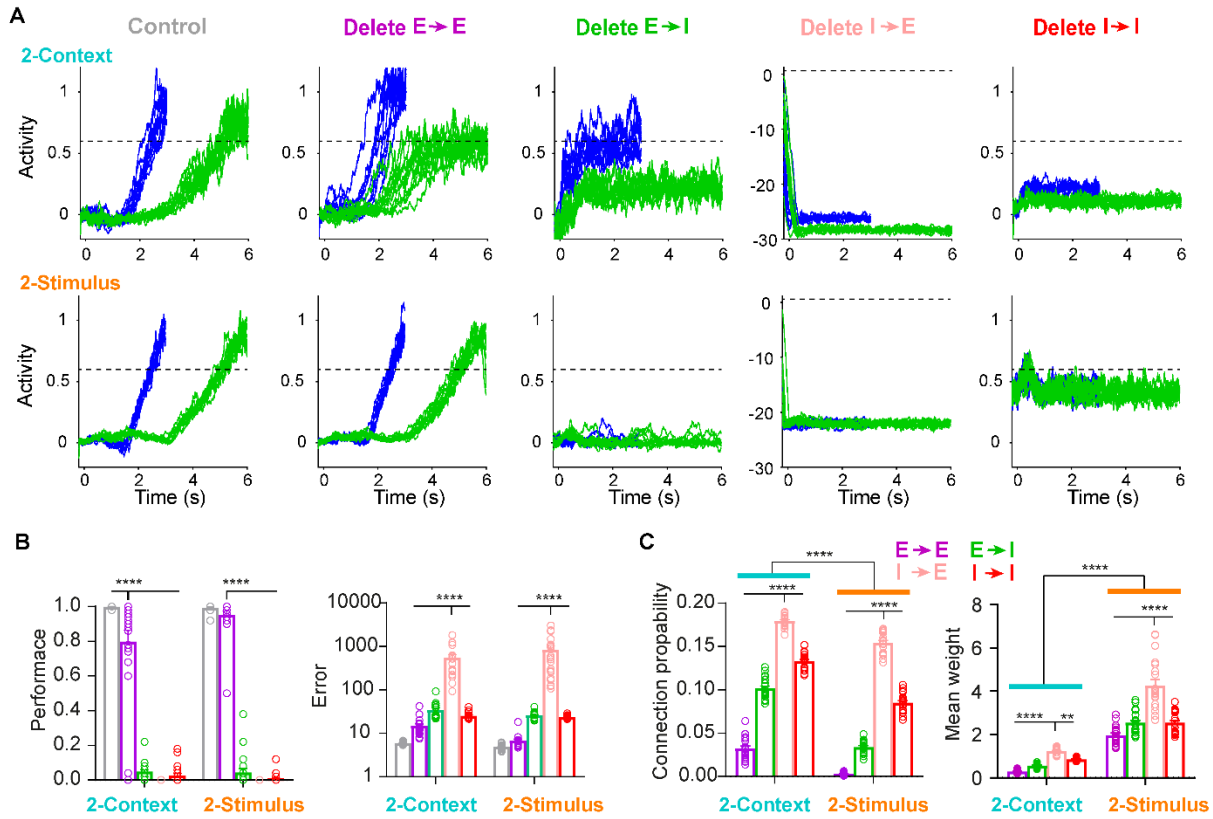


Fig 6. Differential connectivity patterns in RNNs trained on the 2-Context and 2-Stimulus tasks (A) Example of the effects of deleting entire subgroups of synapses on performance in the 2-Context (top) and 2-Stimulus (bottom) tasks. From left to right, example output traces of the short (blue) and long (green) intervals for the control condition, and after deleting all excitatory unit to excitatory unit connections (Delete E→E), all excitatory unit to inhibitory unit connections (Delete E→I), all inhibitory to excitatory unit connections (Delete I→E), and all inhibitory unit to inhibitory unit connections (Delete I→I). **(B)** Mean performance (left) and error (right) of the outputs corresponding to the conditions in panel A. The performance for the Delete E→E condition is significantly lower than the control but significantly higher than the other conditions in 2-Context task. For the 2-Stimulus task performance for Delete E→E was not significantly worse than the control, but significantly higher than the other conditions (two-way ANOVA with mixed-effect design, $F_{4,152} = 823.9$, $P < 0.0001$, posthoc Tukey tests $P < 0.0001$). The error for Delete I→E condition is significantly higher than the other conditions in both 2-Context and 2-Stimulus task (two-way ANOVA with mixed-effect design, $F_{4,152} = 39.8$, $P < 0.0001$, posthoc Tukey tests $P < 0.0001$). **(C)** Left, connection probability in the 2-Context task was significantly higher than in the 2-Stimulus task (two-way ANOVA with mixed-effect design, $F_{1,38} = 338.3$, $P < 0.0001$ for the task factor). Probability for the I→E connections is significantly higher than that for the other three conditions: E→E, E→I, I→I in both 2-Context and 2-Stimulus task ($F_{3,114} = 2884$, $P < 0.0001$ for the connection factor, posthoc Tukey tests $P < 0.0001$). Right, the mean weight in the 2-Context task is significantly lower than that in the 2-Stimulus task (two-way ANOVA with mixed-effect design, $F_{1,38} = 219.1$, $P < 0.0001$ for the task factor). Probability for the I→E connection is significantly higher than that for the other three conditions: E→E, E→I, I→I in both 2-Context and 2-Stimulus task ($F_{3,114} = 183.7$, $P < 0.0001$ for the connection factor, posthoc Tukey tests). ****= $P < 0.0001$, and **= $P = 0.002$.

362 Interestingly, deleting all E→E connections only slightly affected the performance and error for
363 both tasks, while deleting all other three groups decreased the performance or increased the error.
364 Deleting the I→E connections produced the largest change in error (Fig 6B). We next quantified
365 the connection probability and mean weights of each group (Fig 6C). Consistent with the
366 performance and error results, I→E connections exhibited the highest connection probability and
367 mean weights for both tasks. Interestingly, to achieve similar output performance, the two tasks
368 seemed to rely on different strategies in the structural level: 2-Context task favored higher
369 connection probability, while 2-Stimulus task preferred higher mean weights (Fig 6C).

370

371 **RNNs trained for the 2-Stimulus task are more robust to noise**

372 We have seen that RNNs trained for the 2-Context task are better suited for generalization
373 to novel intervals and this feature is related to the underlying dynamics being governed by a
374 absolute-scaling encoding scheme. A question that emerges from these results is whether there is
375 a computational tradeoff between the distinct dynamic regimes observed in both tasks? For
376 example, while the RNNs trained on the 2-Context task exhibit better generalization, do they
377 perform worse on any other measures? As a first step to address this question we analyzed the
378 robustness of both tasks in response to noise. In the brain, of course, neural networks are
379 continuously subject to extraneous noise, and thus robustness to noise imposes an important
380 constraint on biologically functional dynamic regimes [32]

381 As above we first trained RNNs on either the 2-Context and 2-Stimulus tasks with the
382 standard settings, namely noise level of 0.45 (σ in Eq. 1), then we tested the networks by applying
383 different values of σ . Example output traces for the 2-Stimulus task under all noise levels tested
384 were less scattered than that for the 2-Context (Fig 7A). This was supported by the fact that the

385 mean error for the 2-Stimulus task was lower than that for the 2-Context (Fig 7B). For both tasks,
 386 at high noise levels, there were some incorrect trials (< 10% and no significant difference between
 387 the two tasks) in which either the output never crossed the threshold during the trial or crossed the
 388 threshold outside of the acceptance windows We then directly contrasted the temporal precision
 389 of the correct trials and found that the standard deviations for the 2-Stimulus task were lower than
 390 that for the 2-Context task (Fig 7C). Taken together, we conclude that the dynamic regimes
 391 underlying timing in the predominately stimulus-specific dynamics that emerged in the 2-Stimulus
 392 task provided a computational benefit in terms of robustness to noise suggesting computational
 393 tradeoffs between different dynamic regimes for the encoding of time.

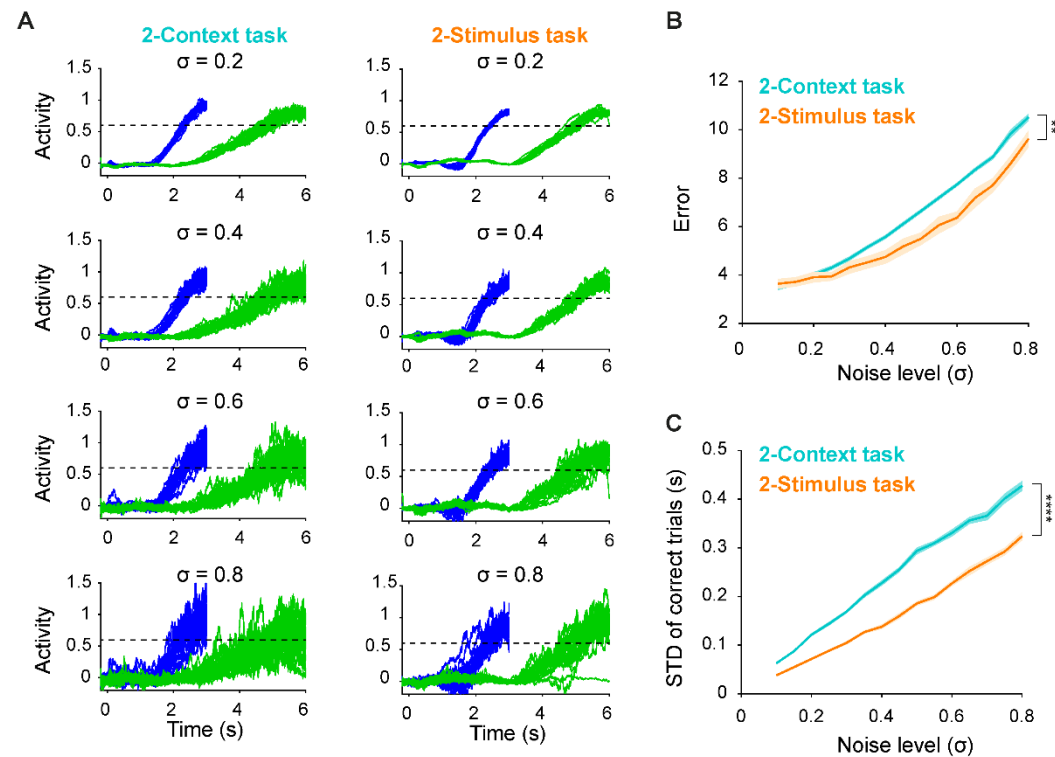


Fig 7. RNNs trained on the 2-Stimulus task were less sensitive to noise perturbations. (A) Output traces for short (blue) and long (green) intervals from an example RNN trained on the 2-Context (left) and 2-Stimulus (right) across different levels of noise (σ) during testing. (B) Mean error (across 50 trials) for 2-Context task (cyan) is higher than that for 2-Stimulus task (orange) ($n = 20$ simulations, two-way ANOVA with mixed-effect design, $F_{1,38} = 9.35$, $P = 0.004$). (C) Mean standard deviation of the time of threshold-crossing across all correct trials for 2-Context task (cyan) is higher than that for 2-Stimulus task (orange) ($F_{1,38} = 341$, $P < 0.0001$). Data are presented as mean \pm SEM.

395 Similar to the generalization performance, the difference of the robustness to noise between
396 the 2-Context and 2-Stimulus tasks was consistent across different input parameters (S1 Fig F),
397 initial gain (S4 Fig D), and connection probability (S5 Fig D) of the recurrent weights.

398

399

400 **Discussion**

401 Here we trained supervised RNNs on two simple temporal tasks that required the production of
402 identical temporal output patterns based on previous behavioral results [14, 18, 23]: a ramping
403 increase in output firing rate that peaked after either a short (3 s) or long (6 s) interval. The tasks
404 differed only in how the short and long intervals were cued: either by a continuously presented
405 context input (2-Context task) or by two distinct brief inputs (2-Stimulus task). In principle the
406 same dynamic regimes could have emerged and solved both tasks, yet, significantly different
407 dynamic regimes emerged in the different tasks. Thus depending on the task RNNs encoded time
408 in different ways, and exhibited fundamentally different computational properties, particularly
409 regarding how the networks generalized to novel stimuli.

410

411 **Neural dynamic regimes of population clocks**

412 A converging body of experimental and computational evidence suggests that neural
413 circuits encode time in spatiotemporal patterns of neural activity. Two experimentally relevant
414 neural dynamics regimes by which neurons can encode time include ramping activity and
415 population clocks. Ramping codes generally refer to monotonically increasing (or decreasing)
416 firing rates throughout an interval [24, 33-40]—in ramping codes firing rate often peaks at the time
417 of the target interval, and in principle, a single neuron can encode time throughout the entire

418 duration. Population clocks refer to time-varying patterns of activity in which time is encoded in
419 the population activity of neurons, which generally exhibit nonmonotonic changes in firing rate,
420 and importantly these dynamics are generated by the recurrent connectivity within a neural circuit
421 [1, 11, 41, 42]. Population clocks can include simple sparse neural sequences as well as complex
422 spatiotemporal patterns in which a given neuron can exhibit multiple time fields [28, 43-51].

423 In the current simulations, the target output patterns were a simple ramping pattern, yet
424 most of the units in the RNNs were not well described as ramping units—even though it seems
425 that this would be the simplest and most direct solution to solve the tasks. Rather, the neural
426 dynamics observed in the RNNs studied here, are most consistent with the notion of population
427 clocks in general and neural sequences in particular (Fig 4). These results are in line with other
428 computational models in which neural sequences encode time [52-55]. The reason RNNs trained
429 with supervised learning rules seem to converge to neural sequences rather than ramping activity
430 are not well understood, but it has been recently proposed that neural sequences represent a fairly
431 optimal encoding scheme for downstream neuron (the output unit in our case) to read out time
432 [23].

433

434 **Absolute, scaling, and stimulus-specific codes**

435 We outlined three general temporal encoding strategies by which a population of neurons
436 could solve temporal tasks that require producing multiple intervals (Fig 3)—such as the two tasks
437 examined here. The scaling strategy is perhaps the most intuitive because it essentially exploits
438 the same neural dynamics to produce both a short or long interval by altering the speed at which
439 the dynamics unfold. Indeed, such scaling has been observed experimentally [14, 16, 23, 26, 38,
440 56, 57]. Neurons that exhibit absolute timing have also been experimentally observed, along with

441 neurons that categorically detect the midpoint boundary between short and long intervals [14, 23,
442 26, 27, 56-61]. Stimulus-specific codes in which the same or different intervals can be encoded in
443 different neural trajectories have also been described [17, 47, 58, 62-64]. To date, however, these
444 different encoding strategies have not been carefully analyzed or quantified. To this end, we
445 described two general purpose quantitative measures—the ASI and SSI_{unit} —that can be applied
446 across a wide range of single-unit data and used to classify neural responses.

447 These measures revealed a different distribution of unit types across the RNNs trained on
448 the 2-Context and 2-Stimulus tasks (Fig 5). Specifically, over 50% of the units in the 2-Context
449 RNNs were classified as scaling units, whereas in the 2-Stimulus RNNs over 50% were classified
450 as stimulus-specific units—that is, their temporal profiles between the short and long interval were
451 not consistent with either absolute or scaling coding strategies. This differential distribution is
452 consistent with the intuition that because in the 2-Context task the context input is active during
453 both the short and long intervals, and a stimulus-specific encoding strategy is more difficult to
454 implement compared to the 2-Stimulus task—i.e., the input space of the 2-Context task is smaller.
455 Put another way, in the 2-Stimulus task RNNs are likely to begin their trajectories at the beginning
456 of each trial ($t=0$) in more distant regions of neural state space than in the 2-Stimulus task.

457 The differential distribution of scaling, absolute, and stimulus-specific neurons accounts in
458 part for the distinct computational features of both types of networks. Specifically, the
459 classification of units into different temporal coding strategies allowed us to demonstrate that
460 selectively deleting some classes impaired RNN performance more than others. Deleting a few
461 inhibitory scaling units impaired RNN performance in the 2-Context task significantly more than
462 deleting absolute or stimulus-selective units. In contrast in the 2-Stimulus task, all classes

463 contributed to performance with an approximately equal weighting—reflecting a much more
464 mixed encoding strategy [65, 66].

465

466 **Computational trade-offs between time-encoding dynamic regimes**

467 The 2-Context and 2-Stimulus tasks required producing the same temporal output patterns
468 but generated dramatically different behaviors when challenged with novel inputs. Of particular
469 relevance was that in response to novel levels of activation of the inputs, the 2-Context RNN
470 exhibited a smooth scaling of the temporal profile of the output. In this task, in response to the *go*
471 stimulus, RNN’s generated a neural trajectory that resembled a neural sequence. Depending on the
472 analog value of the context input this trajectory unfolded at either a slow or fast speed to produce
473 the short or long interval, respectively. Critically, in response to novel levels of activation of the
474 tonic context input the velocity of the neural trajectory varied smoothly—thus generating smooth
475 temporal scaling of the output pattern. This same property has been observed in numerous other
476 models of timing [12, 30, 34, 67-69]. Specifically, a single input or variable is able to modulate
477 the velocity of the RNN dynamics in an approximately linear fashion.

478 In contrast to the temporal scaling behavior observed in the RNN trained on the 2-Context
479 task, when the 2-Stimulus RNNs were tested with inputs they were not trained on (e.g., 50% Input
480 1 + 50% Input 2) they did not exhibit smooth generalization. Importantly, they also did not exhibit
481 catastrophic degradation—i.e., the internal dynamics was robust to very different initial states.
482 Rather they exhibited categorical timing—essentially a winner-take-all competition between two
483 distinct trajectories. This result is consistent with the notion that RNNs can encode multiple neural
484 trajectories in regimes that have been referred to as dynamic attractors [31, 70], locally stable
485 transient trajectories [71, 72], or stable heteroclinic channels [73, 74]. Here, two trajectories

486 possess their own basins of attraction (or “rivers-of-attraction”) which lead the activity of the
487 network into one or the other of the two dynamic attractors.

488 Both temporal scaling and categorical timing are behaviorally relevant forms of timing.
489 Specifically, some tasks require smoothly scaling the temporal output patterns, while others
490 require categorically discriminating or producing one of distinct two intervals [12-15, 21, 22].
491 Thus, we have shown that the population clocks that emerge in RNNs can account for both
492 temporal scaling and categorical timing and that it is possible to distinguish between both regimes
493 based on the percentage of units that undergo scaling or stimulus-specific timing.

494 It is also relevant to note that RNNs learned to solve the 2-Context task in fewer training
495 trials than the 2-Stimulus task. This may be because it is easier to adjust weights to generate a
496 single trajectory at two different speeds than to generate largely distinct trajectories. Furthermore,
497 during training the 2-Context task the RNN is always subject to tonic external input which in effect
498 might facilitate learning by suppressing the potential emergence of chaotic regimes [75, 76].

499

500 **Experimental predictions**

501 As is evident from the behavioral data, a wide range of distinct neural regimes, from
502 ramping activity to a diverse range of neural population clocks, have been observed experimentally
503 across different brain areas and behavioral tasks [for reviews see: 1, 6, 7, 10]. Here we show that
504 the same is true even in RNNs trained on two tasks that require the production of the same temporal
505 output patterns. Our results thus suggest that much of the experimentally observed variability
506 might be accounted for by relatively subtle differences in task structure. Furthermore, because
507 most timing tasks used in laboratories tap into ecologically relevant behaviors, different tasks may
508 encourage generalization patterns that best approximate their ecological relevance. These distinct

509 generalization patterns will, in turn, result in time being encoded in different dynamic regimes—
510 e.g., regimes that are well-suited for temporal scaling or categorical timing.

511 A number of strong experimental predictions emerge from our results. First, at the
512 behavioral level, we predict that whether rodents are trained on the 2-Context or 2-Stimulus will
513 lead to different generalization patterns to novel stimuli. For example, a single odor along with a
514 tone context stimulus could be used for the 2-Context task, and two brief odors as the stimuli in
515 the 2-Stimulus task. We predict that changing the loudness of the tone in the 2-Context task will
516 scale the output pattern, but mixing the odors will result in categorical timing rather than the
517 production of an intermediary interval. Second, we predict that neural recordings from animals
518 trained on these tasks will exhibit specific neural dynamic signatures, i.e., in the 2-Context task
519 more neurons will be categorized as scaling units compared to the 2-Stimulus task. Of course, one
520 must take into account that results may be dependent on the brain areas being recorded. However,
521 based on the current literature we expect this prediction to hold in those areas that have been
522 implicated in timing across many tasks, including the striatum, supplementary/secondary motor
523 areas, and prefrontal cortical areas.

524

525 **Materials and Methods**

526 **Firing-rate RNN model**

527 RNNs were based on firing-rate units that obeyed Dale’s law ($N = 200$, 80/20%
528 excitatory/inhibitory). RNN dynamics was described by the following equations:

529

$$530 \quad \tau \frac{dx}{dt} = -x + \mathbf{W}^{rec} * \mathbf{r} + \mathbf{W}^{in} * \mathbf{I} + \sigma * \mathbf{N}(0,1) * \sqrt{2 * \tau} \quad (1)$$

531

$$532 \quad o = \mathbf{W}^{out} * \mathbf{r} \quad (2)$$

533

$$534 \quad \mathbf{r} = \min(\ln(1 + e^x), 20) \quad (3)$$

535

536 where $\mathbf{x} \in \mathbb{R}^{N \times 1}$ represents the input currents of RNN units, and firing rate vector \mathbf{r} is obtained by
537 applying a Softplus function constrained by an upper bound of 20. The time constant τ was equal
538 to 100 ms for all units. $\mathbf{W}^{in} \in \mathbb{R}^{N \times 2}$ and \mathbf{I} are the input weights and external inputs, which are task-
539 specific as described below. Each unit received independent Gaussian noise $\mathbf{N}(0,1)$ with the
540 standard deviation of $\sigma\sqrt{2\tau}$. Unless otherwise specified, $\sigma = 0.45$. $\mathbf{W}^{rec} \in \mathbb{R}^{N \times N}$ is the recurrent
541 weight matrix. Self-connections were absent in the network. The output (o) of the network is
542 computed linearly from the output weights \mathbf{W}^{out} and \mathbf{r} . RNNs were implemented and trained in
543 Tensorflow starting from the code of Kim et al [77, 78].

544 *Training.* Networks were trained using adaptive moment estimation stochastic gradient
545 descent algorithm (Adam) to minimize the error between network output o and target z :

546

547
548
549
550
551
552
553
554
555
556
557
558
559
560
561
562
563
564
565
566
567

$$Error = \sqrt{\sum_{t=0}^T [o(t) - z(t)]^2} \quad (4)$$

where T is the total length of a given trial. The target and mask are task-dependent as described below. The learning rate was 0.01, and other TensorFlow default values were used.

Only recurrent weights \mathbf{W}^{rec} and output weights \mathbf{W}^{out} were trained. Unless otherwise specified, \mathbf{W}^{rec} was initialized as a random sparse matrix with a connection probability of 0.2 from a normal distribution with zero mean and standard deviation (gain) of 1 and transformed to absolute values. To begin in an approximately balanced regime the inhibitory weights were multiplied by 4 for the initialization but not for training. To respect Dale’s law during training a rectified linear operation was applied on \mathbf{W}^{rec} to clip the weights down to zero and then excitation and inhibition were implemented by multiplying the clipped \mathbf{W}^{rec} with a diagonal matrix of 1 and -1 representing excitatory and inhibitory units, respectively [78, 79]. \mathbf{W}^{in} was drawn from a standard normal distribution and was fixed during training.

During training, a discretization step of 20 ms was used. After training, RNNs were ported to Matlab using the trained parameters and a discretization step of 1ms was used to get the dynamics for analyses.

Parameters were updated every trial. After every 100 trials of training, the network was tested for 100 trials to compute the task performance (see below) and mean error. When task performance was higher than 97% and the mean error is lower than 2, the training was considered a success and stopped

568 Interval tasks

569 *2-Context task.* unless otherwise specified, inspired by the timing task used by previous
 570 works [14, 18] in which context cues indicated the lengths of intervals, we designed a 2-Context
 571 two-interval task. In this task, the output of the RNN needs to generate either a short (3 s) or long
 572 (6 s) interval in each trial. For a given training trial with length T , two external inputs \mathbf{I}_{go}^1 and
 573 $\mathbf{I}_{context}^2$ were applied at $stim_{onset}$ after a baseline with random durations between 0.2 and 0.6 s.
 574 Specifically,

$$575 \quad I_{go}(t) = \begin{cases} 1 & stim_{onset} < t \leq (stim_{onset} + 0.5) \\ 0 & otherwise \end{cases} \quad \text{for both short and long trials,}$$

576

$$577 \quad I_{context}(t) = \begin{cases} 0.75 \text{ or } 0.25 & stim_{onset} < t \leq T, \text{ for short or long trials repectively} \\ 0 & otherwise \end{cases}$$

578

579 The output targets were defined as:

$$580 \quad z(t) = \begin{cases} \frac{t - stim_{onset} - 0.5 * Int_{target}}{0.5 * Int_{target}} & (stim_{onset} + 0.5 * Int_{target}) < t \leq (stim_{onset} + Int_{target}) \\ 1 & (stim_{onset} + Int_{target}) < t \leq (stim_{onset} + Int_{target} + 0.2) \\ 0 & otherwise \end{cases}$$

581 where the target intervals (Int_{target}) were 3 and 6 seconds for the short and long trials, respectively.

582 *2-Stimulus task.* unless otherwise specified, the 2-Stimulus task was based on a two-
 583 interval odor discrimination task [23], which required the production of the identical output
 584 patterns as the 2-Context task. However, the short and long intervals were cued by two different
 585 inputs \mathbf{I}_{short} and \mathbf{I}_{long} which like the \mathbf{I}_{go} in the 2-Context task stepped up from 0 to 1 for a brief 0.5
 586 s period.

587 *Task performance.* Response time for a given trial was defined as the time when the output
 588 crosses a threshold of 0.6. The correct trials were defined as those in which the output crossed the

589 threshold within an acceptance window between $\text{stim}_{\text{onset}} + 0.5 \text{Int}_{\text{target}}$ and $\text{stim}_{\text{onset}} + \text{Int}_{\text{target}}$. Task
590 performance was defined as the ratio of correct trials among all testing trials.

591 Unless otherwise specified, the “delay” epoch ($\text{stim}_{\text{onset}}$ to $\text{stim}_{\text{onset}} + \text{Int}_{\text{target}}$) was used for
592 analysis.

593

594 **Generalization to novel inputs**

595 To test how the RNN trained on the 2-Context task would generalize to novel intervals as
596 in Fig 2, we first trained the RNN using the normal setting for the 2-Context task, namely $\mathbf{I}_{\text{context}}$
597 of 0.75 and 0.25 for the short and long trials, respectively. Then we tested the trained RNNs by
598 gradually varying the context level from 0.75 to 0.25 with steps of 0.05. Fifty trials of each level
599 were obtained for analyses.

600 After training in the 2-Stimulus task generalization to novel inputs was tested by gradually
601 varying the ratio of $\mathbf{I}_{\text{short}}$ and \mathbf{I}_{long} with steps of 0.1 so that the sum of both inputs was always 1.

602 *Correlation measure* To quantify changes in the temporal profile of the output units across
603 different inputs during generalization tests we first computed the correlation coefficient between
604 the mean response times (when the output crosses the threshold) and the generalization conditions
605 for both the 2-Context and 2-Stimulus tasks (the absolute values of the correlations were used due
606 to the negative correlation for the 2-Context task).

607 *Sigmoid slope measure.* To further quantify generalization to novel inputs in both tasks we
608 also fitted the mean response times to the input conditions with a sigmoid function as follow:

609

$$y = b + \frac{a - b}{1 + e^{g*(m-x)}}$$

610 Standard nonlinear least square methods implemented in Matlab were used to optimize the fits.
611 We then compared the slope g for both tasks. Higher g values reflect more categorical
612 generalization.

613

614 **Prototypical dynamical regimes for timing two intervals**

615 To illustrate the possible neural dynamical strategies used for timing two intervals—
616 scaling, absolute, and stimulus-specific, we generated three pairs of prototypical dynamics for the
617 short (3 s) and long (6 s) intervals composed of 100 units with the time step of 0.001 s (Fig 3). In
618 such settings, the dynamics for the short and long interval were represented as 100×3000 and
619 100×6000 matrices respectively, with the row being units and column being time points.

620 The dynamics for long interval were the same for all three strategies, which was described
621 as:

$$622 \quad x_i(t) = e^{\frac{-(t - \frac{i}{100} * 6)^2}{2 * 0.8^2}} \text{ for } i = 1, 2, \dots, 100$$

623 where dynamics of all units were Gaussian functions with the same variance but different means
624 uniformly spanned the whole 6 s. The dynamics for the short interval were different for the three
625 strategies and were defined as follows:

626 *Scaling.* The dynamics for the short interval in the scaling strategy was simply a matrix of
627 uniform subsampling of the time dimension of the long dynamics.

628 *Absolute.* For the absolute strategy, the dynamics of the first 50 units for the short interval
629 were the same as that for the long interval.

630 *Stimulus-specific.* For stimulus-specific example, we first uniformly subsampled the time
631 dimension of the long dynamics matrix to 3 s. Then we randomized the order of the unit indices.

632

633 **The stimulus-specific index at the population-level (SSI_{pop})**

634 As in Fig 4, to quantify how well the short and long neural trajectories can be explained by
 635 the stimulus-specific strategy at the population level, we developed a novel stimulus-specific index
 636 in population-level (SSI_{pop}), which is largely based on establishing that the trajectories are not
 637 consistent with temporal scaling or absolute timing. We first obtained the mean population
 638 dynamics ($\Delta t=1$ ms) for two intervals by averaging across 25 trials, which led to two matrices,
 639 $\mathbf{X}_{\text{short}}$ (200×3000) and \mathbf{X}_{long} (200×6000). We computed the pairwise Euclidean distance between
 640 $\mathbf{X}_{\text{short}}$ and \mathbf{X}_{long} , which led to the distance matrix \mathbf{D} (3000×6000). We then obtained the index of
 641 the minimum values across each row of \mathbf{D} , which led to the minimal distance vector \mathbf{I}_{min} (3000×1),
 642 which partially captures the relationship between the population dynamics for the short and long
 643 intervals.

644 Next \mathbf{I}_{min} was contrasted with a reference matrix \mathbf{R} (3000×3000) with τ indexing the
 645 column:

$$646 \begin{bmatrix} 1 & 1 & 1 & 1 & \dots & 1 & 1 & 1 \\ 3 & 2 & 2 & 2 & \dots & 2 & 2 & 2 \\ 5 & 4 & 3 & 3 & \dots & 3 & 3 & 3 \\ 7 & 6 & 5 & 4 & \dots & 4 & 4 & 4 \\ \dots & \dots \\ \dots & \dots \\ 5998 & 5998 & 5998 & 5998 & \dots & 4499 & 2999 & 2999 \\ 6000 & 6000 & 6000 & 6000 & \dots & 6000 & 6000 & 3000 \end{bmatrix}$$

647 Specifically, a given column vector corresponding to τ in \mathbf{R} is defined as:

$$648 [1, 2, 3, \dots, \tau, \tau + \alpha, \tau + 2\alpha, \tau + 3\alpha, \dots, \tau + (3000 - \tau)\alpha]$$

$$649 \alpha = \frac{6000 - \tau}{3000 - \tau}, \quad \tau = 1, 2, 3, \dots, 2999$$

650 Each column vector (3000×1) in \mathbf{R} represents one absolute-scaling reference profile spanning from
651 pure scaling ($\tau = 1$) to pure absolute ($\tau = 3000$), with mixed profiles in between in which absolute
652 timing transitions to scaling at τ with the scaling factor α varied to keep the length of each vector
653 the same. We then computed the Euclidian distances between \mathbf{I}_{\min} and all the column vectors of \mathbf{R}
654 and extracted the vector with the minimum distance at τ_{\min} , which indicates the best reference
655 vector that can be used to explain the \mathbf{I}_{\min} . Note that the construction of the \mathbf{R} matrix accounts for
656 units that fire throughout the entire trial—thus capturing the properties of a neuron that always
657 fired at the end of the trial (e.g., a potential motor neuron). It is also possible to build \mathbf{R} by fixing
658 the scaling factor at 2 after each point τ , in which case the last element of each column in \mathbf{R} would
659 progressively change from 6000 to 3000. We have run analyses with this partial scaling approach
660 as well with qualitatively similar results.

661 Finally, the SSI_{pop} was defined as:

$$662 \quad SSI_{\text{pop}} = 1 - c(\tau_{\min}).$$

663 where the $c(\tau_{\min})$ is the correlation between the \mathbf{I}_{\min} and the reference vector at τ_{\min} . For pure scaling
664 dynamics for the two intervals as an example, \mathbf{I}_{\min} should be the main diagonal of distance matrix
665 \mathbf{D} , [1, 3, 5, 7, ..., 6000], which makes $\tau_{\min} = 1$, corresponding to the pure scaling reference vector.
666 Consequently, the $c(\tau_{\min})$ is 1 and SSI_{pop} is 0. That indicates that the pure scaling dynamics can not
667 be explained by stimulus-specific strategy but by absolute-scaling strategies, in which the
668 dynamics of the short and long interval relate to each other in a way of absolute or scaling or mixed
669 of both (see below for the absolute-scaling index at the single-unit level)

670

671 **Stimulus-specific index and absolute-scaling index (ASI) for single**
672 **units**

673 We extended a previous description of an absolute vs. scaling index (ASI) for single units
674 [23], by including a novel measure of the stimulus-specific profile: the stimulus-specific index at
675 the single-cell level (SSI_{unit} as in Fig 5A). As described previously we searched for the best
676 transformation of dynamics for the long interval ($y(t)$) to that for the short interval ($x(t)$), by
677 concatenating an absolute portion of the long response ($y^{abs}(t)$) and a temporally scaled portion of
678 the long response scaled by a factor α ($y^{scale}(t')$). More specifically, we searched for a breakpoint
679 τ to divide $y(t)$ into an absolute and scaled segment, that best matches $x(t)$, as measured by the
680 Euclidean distance ($Dist(\tau)$). Specifically,

$$681 \quad \alpha = (T_{long} - \tau) / (T_{short} - \tau)$$

$$682 \quad Dist(\tau) = \sqrt{\sum_{t=0}^{\tau} (x(t) - y(t))^2 + \sum_{t=\tau}^{T_{short}} (x(t) - y(\tau + \alpha(t - \tau)))^2}$$

$$683 \quad \tau_{min} = argmin_{\tau}(Dist(\tau))$$

$$684 \quad Corr(\tau_{min})$$

$$685 \quad = \frac{\sum_{t=0}^{\tau_{min}} (x(t) - \bar{x})(y(t) - \bar{y}) + \sum_{t=\tau_{min}}^{T_{short}} (x(t) - \bar{x})[y(\tau_{min} + \alpha(t - \tau_{min})) - \bar{y}]}{\sqrt{\sum_{t=0}^{T_{short}} (x(t) - \bar{x})^2} \sqrt{\sum_{t=0}^{\tau_{min}} (y(t) - \bar{y})^2 + \sum_{t=\tau_{min}}^{T_{short}} (y(\tau_{min} + \alpha(t - \tau_{min})) - \bar{y})^2}}$$

$$686 \quad SSI_{unit} = 1 - Corr(\tau_{min}).$$

$$687 \quad W^{abs}(\tau_{min}) = 1/N_{1:\tau_{min}} \sum_{t=0}^{\tau_{min}} |[x(t) - x(0)][y(t) - y(0)]|$$

$$688 \quad W^{scale}(\tau_{min}) = 1/N_{\tau_{min}:T_{short}} \sum_{t=\tau_{min}}^{T_{short}} |[x(t) - x(\tau_{min})][y(\tau_{min} + \alpha(t - \tau_{min})) - y(\tau_{min})]|$$

$$689 \quad AbsR(\tau_{min}) = \frac{W^{abs}(\tau_{min})}{W^{scale}(\tau_{min}) + W^{abs}(\tau_{min})}$$

690

691
$$ASI = (\frac{\tau_{min}}{T_{short}} + AbsR(\tau_{min}))/2$$

692 τ spans all possible breakpoints from 0 to T_{short} (for the short interval and T_{long} for the long interval).
693 The segment before τ denotes the absolute period and the period after τ denotes the segment scaled
694 by α for the long response. τ_{min} corresponds to the breakpoint with the minimal Euclidian distance
695 $Dist(\tau_{min})$. Different from previous work [23], we also computed the correlation coefficient
696 between $x(t)$ and transformed $y(t)$, $Corr(\tau_{min})$. Then the SSI_{unit} is defined as that 1 minus $Corr(\tau_{min})$.
697 In the following steps, the absolute and scaling weights are calculated between dynamics for the
698 short interval and the time-warped dynamics for the long interval at τ_{min} with $N_{a:b}$ being the number
699 of time points between a and b, and absolute ratio $AbsR(\tau_{min})$ was also calculated. The absolute
700 temporal factor corresponds to τ_{min} / T_{short} , and ASI was defined as the average of the absolute
701 temporal factor and the $AbsR(\tau_{min})$.

702 To classify each unit as a stimulus-specific, scaling, or absolute unit we first calculated
703 SSI_{unit} for each unit. We then classified a unit as stimulus-specific if SSI_{unit} was > 0.5 ; if the SSI_{unit}
704 was ≤ 0.5 then looked at its ASI and classified it as an absolute unit if $ASI > 0.5$, or as a scaling
705 unit if $ASI \leq 0.5$.

706

707 **Unit-deletion and weight deletions experiments**

708 Based on the classification of units being stimulus-specific, scaling, or absolute, we ran
709 deletion experiments to start to understand the causal role of each type of unit (S6 Fig). For a given
710 unit to be deleted, we removed all the connections attached to that unit in connection matrix \mathbf{W}^{rec}
711 as in Eq. 1 and then ran the RNN with the rest parameters fixed. We tested various numbers of
712 deleted units in each type. For a given condition, we randomly selected the deleted cells from the

713 pool 10 times and repeated each deletion experiment for 20 trials for each interval. Then
714 performance and error were averaged across all selections and trials.

715 To quantify how much each class of connection types— $E \rightarrow E$, $E \rightarrow I$, $I \rightarrow E$ and $I \rightarrow I$
716 connections—contributed to the recurrent dynamics and output performance, we performed
717 synapse deletion experiments. Similar to the unit deletions, for a specific class of connections, we
718 set all the weights of that group to be zeros while leaving the other weights unchanged.
719 Performance and error were then computed for each condition (Fig 6).

720

721 **Pairwise angle analysis**

722 To understand the relationships between the RNNs trained on 2-Context and 2-Stimulus
723 task and the input/output subspace (S7 Fig) defined by the inputs weights and output weights, we
724 first performed principal component analysis (PCA) on the concatenated mean dynamics for the
725 short and long intervals. We then projected the original dynamics into the first three PCs. We then
726 binned the projected dynamics into segments of 250 ms. For a given segment, a vector was
727 obtained by subtracting its start point from its end point. Finally, we computed the pairwise angles
728 between all such segment vectors across time and projections of the input/output weight vectors
729 in the same PC space.

730

731 **Noise perturbation experiments**

732 As in Fig 7, to test the robustness of the outputs of the RNN trained on the 2-Context and
733 2-Stimulus tasks, we first trained the two tasks with noise level $\sigma = 0.45$ as in equation (1). We
734 then tested the trained RNNs with various levels σ from 0.1 to 0.8 for 50 trials for each interval.
735 We then compared the error between the outputs and targets for all trials and the standard deviation

736 of the crossing times for the correct trials. Note that for all conditions tested, the incorrect trials
737 were less than 10% for both tasks, and there was no significant difference for that between the two
738 tasks.

739

740 **Statistical analyses**

741 Statistical analyses were carried out with standard functions in MATLAB (MathWorks)
742 and Prism (GraphPad Software). The sample size, type of test, P values, and the F values for
743 ANOVA are indicated in the figure legends. All data and error bars represent the mean and SEM
744 except for the boxplot in Fig 4, where median and quartiles were presented. In all figures, the
745 convention is *: $P < 0.05$, **: $P < 0.01$, ***: $P < 0.001$, ****: $P < 0.0001$.

746

- 748 1. Paton JJ, Buonomano DV. The Neural Basis of Timing: Distributed Mechanisms for Diverse
749 Functions. *Neuron*. 2018;98(4):687-705. doi: <https://doi.org/10.1016/j.neuron.2018.03.045>. PubMed
750 PMID: 29772201; PubMed Central PMCID: PMC5962026.
- 751 2. Buhusi CV, Meck WH. What makes us tick? Functional and neural mechanisms of interval timing.
752 *Nat Rev Neurosci*. 2005;6(10):755-65. doi: 10.1038/nrn1764. PubMed PMID: 16163383.
- 753 3. Meck WH, Ivry RB. Editorial overview: Time in perception and action. *Current Opinion in*
754 *Behavioral Sciences*. 2016;8:vi-x. doi: <https://doi.org/10.1016/j.cobeha.2016.03.001>.
- 755 4. Cannon JJ, Patel AD. How Beat Perception Co-opts Motor Neurophysiology. *Trends in Cognitive*
756 *Sciences*. 2021;25(2):137-50. doi: <https://doi.org/10.1016/j.tics.2020.11.002>.
- 757 5. Coull JT, Nobre AC. Where and When to Pay Attention: The Neural Systems for Directing
758 Attention to Spatial Locations and to Time Intervals as Revealed by Both PET and fMRI. *The*
759 *Journal of Neuroscience*. 1998;18(18):7426-35.
- 760 6. Merchant H, Harrington DL, Meck WH. Neural Basis of the Perception and Estimation of Time.
761 *Annual Review of Neuroscience*. 2013;36(1):313-36. doi: doi:10.1146/annurev-neuro-062012-
762 170349. PubMed PMID: 23725000.
- 763 7. Issa JB, Tocker G, Hasselmo ME, Heys JG, Dombeck DA. Navigating Through Time: A Spatial
764 Navigation Perspective on How the Brain May Encode Time. *Annual Review of Neuroscience*.
765 2020;43(1):null. doi: 10.1146/annurev-neuro-101419-011117. PubMed PMID: 31961765.
- 766 8. Coull JT, Cheng R-K, Meck WH. Neuroanatomical and Neurochemical Substrates of Timing.
767 *Neuropsychopharmacology*. 2011;36(1):3-25.
- 768 9. Buonomano DV, Karmarkar UR. How do we tell time? *Neuroscientist*. 2002;8(1):42-51. doi:
769 10.1177/107385840200800109. PubMed PMID: 11843098.
- 770 10. Fung BJ, Sutlief E, Hussain Shuler MG. Dopamine and the interdependency of time perception and
771 reward. *Neuroscience & Biobehavioral Reviews*. 2021;125:380-91. doi:
772 <https://doi.org/10.1016/j.neubiorev.2021.02.030>.
- 773 11. Buonomano DV, Laje R. Population clocks: motor timing with neural dynamics. *Trends in*
774 *Cognitive Sciences*. 2010;14(12):520-7.
- 775 12. Hardy NF, Goudar V, Romero-Sosa JL, Buonomano DV. A model of temporal scaling correctly
776 predicts that motor timing improves with speed. *Nature Communications*. 2018;9(1):4732. doi:
777 10.1038/s41467-018-07161-6. PubMed Central PMCID: PMC6226482.
- 778 13. Slayton MA, Romero-Sosa JL, Shore K, Buonomano DV, Viskontas IV. Musical expertise
779 generalizes to superior temporal scaling in a Morse code tapping task. *PLOS ONE*.
780 2020;15(1):e0221000. doi: 10.1371/journal.pone.0221000.
- 781 14. Wang J, Narain D, Hosseini EA, Jazayeri M. Flexible timing by temporal scaling of cortical
782 responses. *Nature Neuroscience*. 2018;21(1):102-10. doi: 10.1038/s41593-017-0028-6.
- 783 15. Lerner Y, Honey CJ, Katkov M, Hasson U. Temporal scaling of neural responses to compressed and
784 dilated natural speech. *Journal of Neurophysiology*. 2014;111(12):2433-44. doi:
785 10.1152/jn.00497.2013.
- 786 16. Mello GBM, Soares S, Paton JJ. A scalable population code for time in the striatum. *Curr Biol*.
787 2015;9:1113-22.
- 788 17. Shimbo A, Izawa E-I, Fujisawa S. Scalable representation of time in the hippocampus. *Science*
789 *Advances*. 2021;7(6):eabd7013. doi: 10.1126/sciadv.abd7013.
- 790 18. Kunitatsu J, Suzuki TW, Ohmae S, Tanaka M. Different contributions of preparatory activity in the
791 basal ganglia and cerebellum for self-timing. *Elife*. 2018;7. doi: 10.7554/eLife.35676. PubMed
792 PMID: 29963985; PubMed Central PMCID: PMC6050043.

- 793 19. Aasland WA, Baum SR. Temporal parameters as cues to phrasal boundaries: A comparison of
794 processing by left- and right-hemisphere brain-damaged individuals. *Brain and Language*.
795 2003;87(3):385-99. doi: 10.1016/S0093-934X(03)00138-X.
- 796 20. Schwab S, Miller JL, Grosjean F, Mondini M. Effect of Speaking Rate on the Identification of Word
797 Boundaries. *Phonetica*. 2008;65(3):173-86.
- 798 21. Kim J, Ghim J-W, Lee JH, Jung MW. Neural Correlates of Interval Timing in Rodent Prefrontal
799 Cortex. *The Journal of Neuroscience*. 2013;33(34):13834-47. doi: 10.1523/jneurosci.1443-13.2013.
- 800 22. Allan LG, Gibbon J. Human bisection at the geometric mean. *Learning and Motivation*. 1991;22(1-
801 2):39-58.
- 802 23. Zhou S, Masmanidis SC, Buonomano DV. Neural Sequences as an Optimal Dynamical Regime for
803 the Readout of Time. *Neuron*. 2020;108(4):651-8.e5. doi:
804 <https://doi.org/10.1016/j.neuron.2020.08.020>.
- 805 24. Leon MI, Shadlen MN. Representation of time by neurons in the posterior parietal cortex of the
806 macaque. *Neuron*. 2003;38:317-27.
- 807 25. Gouvea TS, Monteiro T, Motiwala A, Soares S, Machens C, Paton JJ. Striatal dynamics explain
808 duration judgments. *Elife*. 2015;4. doi: 10.7554/eLife.11386. PubMed PMID: 26641377; PubMed
809 Central PMCID: PMC4721960.
- 810 26. Emmons EB, De Corte BJ, Kim Y, Parker KL, Matell MS, Narayanan NS. Rodent Medial Frontal
811 Control of Temporal Processing in the Dorsomedial Striatum. *The Journal of Neuroscience*.
812 2017;37(36):8718-33. doi: 10.1523/jneurosci.1376-17.2017.
- 813 27. Merchant H, Zarco W, Pérez O, Prado L, Bartolo R. Measuring time with different neural
814 chronometers during a synchronization-continuation task. *Proceedings of the National Academy of
815 Sciences*. 2011;108(49):19784-9. doi: 10.1073/pnas.1112933108.
- 816 28. Crowe DA, Zarco W, Bartolo R, Merchant H. Dynamic Representation of the Temporal and
817 Sequential Structure of Rhythmic Movements in the Primate Medial Premotor Cortex. *The Journal
818 of Neuroscience*. 2014;34(36):11972-83. doi: 10.1523/jneurosci.2177-14.2014.
- 819 29. Kraus BJ, Robinson RJ, White JA, Eichenbaum H, Hasselmo ME. Hippocampal “Time Cells”: Time
820 versus Path Integration. *Neuron*. 2013;78(6):1090-101. doi: 10.1016/j.neuron.2013.04.015. PubMed
821 PMID: 23707613; PubMed Central PMCID: PMC3913731.
- 822 30. Remington ED, Narain D, Hosseini EA, Jazayeri M. Flexible Sensorimotor Computations through
823 Rapid Reconfiguration of Cortical Dynamics. *Neuron*. 2018;98(5):1005-19.e5. doi:
824 10.1016/j.neuron.2018.05.020. PubMed PMID: 29879384; PubMed Central PMCID: PMC6009852.
- 825 31. Goudar V, Buonomano DV. Encoding sensory and motor patterns as time-invariant trajectories in
826 recurrent neural networks. *eLife*. 2018;7:e31134. doi: 10.7554/eLife.31134. PubMed PMID:
827 29537963; PubMed Central PMCID: PMC5851701.
- 828 32. Huk AC, Hart E. Parsing signal and noise in the brain. *Science*. 2019;364(6437):236-7. doi:
829 10.1126/science.aax1512.
- 830 33. Liu Y, Tiganj Z, Hasselmo ME, Howard MW. A neural microcircuit model for a scalable scale-
831 invariant representation of time. *Hippocampus*. 2019;29(3):260-74. doi: 10.1002/hipo.22994.
- 832 34. Shankar KH, Howard MW. A Scale-Invariant Internal Representation of Time. *Neural Computation*.
833 2012;24(1):134-93. doi: 10.1162/NECO_a_00212.
- 834 35. Narayanan NS. Ramping activity is a cortical mechanism of temporal control of action. *Current
835 Opinion in Behavioral Sciences*. 2016;8:226-30. doi:
836 <http://dx.doi.org/10.1016/j.cobeha.2016.02.017>.
- 837 36. Durstewitz D. Self-organizing neural integrator predicts interval times through climbing activity. *J
838 Neurosci*. 2003;23(12):5342-53. PubMed PMID: 12832560.
- 839 37. Simen P, Balci F, de Souza L, Cohen JD, Holmes P. A model of interval timing by neural
840 integration. *J Neurosci*. 2011;31(25):9238-53. Epub 2011/06/24. PubMed PMID: 21697374;
841 PubMed Central PMCID: PMC3142662.
- 842 38. Jazayeri M, Shadlen Michael N. A Neural Mechanism for Sensing and Reproducing a Time Interval.
843 *Current Biology*. 2015;25(20):2599-609. doi: 10.1016/j.cub.2015.08.038.

- 844 39. Simen P, Vlasov K, Papadakis S. Scale (In)Variance in a Unified Diffusion Model of Decision
845 Making and Timing. *Psychological Review*. 2016;123(2):151-81. doi: 10.1037/rev0000014. PubMed
846 PMID: WOS:000371141900002.
- 847 40. Finkelstein A, Fontolan L, Economo MN, Li N, Romani S, Svoboda K. Attractor dynamics gate
848 cortical information flow during decision-making. *Nat Neurosci*. 2021;24(6):843-50. doi:
849 10.1038/s41593-021-00840-6. PubMed PMID: 33875892.
- 850 41. Buonomano DV, Mauk MD. Neural network model of the cerebellum: temporal discrimination and
851 the timing of motor responses. *Neural Comput*. 1994;6:38–55.
- 852 42. Medina JF, Garcia KS, Nores WL, Taylor NM, Mauk MD. Timing mechanisms in the cerebellum:
853 testing predictions of a large-scale computer simulation. *J Neurosci*. 2000;20(14):5516-25. PubMed
854 PMID: 10884335.
- 855 43. Lynch Galen F, Okubo Tatsuo S, Hanuschkin A, Hahnloser Richard HR, Fee Michale S. Rhythmic
856 Continuous-Time Coding in the Songbird Analog of Vocal Motor Cortex. *Neuron*. 2016;90(4):877-
857 92. doi: 10.1016/j.neuron.2016.04.021.
- 858 44. Hahnloser RHR, Kozhevnikov AA, Fee MS. An ultra-sparse code underlies the generation of neural
859 sequence in a songbird. *Nature*. 2002;419:65-70.
- 860 45. Long MA, Fee MS. Using temperature to analyse temporal dynamics in the songbird motor pathway.
861 *Nature*. 2008;456(7219):189-94.
- 862 46. Picardo Michel A, Merel J, Katlowitz Kalman A, Vallentin D, Okobi Daniel E, Benezra Sam E, et
863 al. Population-Level Representation of a Temporal Sequence Underlying Song Production in the
864 Zebra Finch. *Neuron*. 2016;90(4):866-76. doi: 10.1016/j.neuron.2016.02.016.
- 865 47. Pastalkova E, Itskov V, Amarasingham A, Buzsaki G. Internally Generated Cell Assembly
866 Sequences in the Rat Hippocampus. *Science*. 2008;321(5894):1322-7. doi:
867 10.1126/science.1159775. PubMed PMID: 18772431; PubMed Central PMCID: PMC2570043.
- 868 48. Carnevale F, de Lafuente V, Romo R, Barak O, Parga N. Dynamic Control of Response Criterion in
869 Premotor Cortex during Perceptual Detection under Temporal Uncertainty. *Neuron*.
870 2015;86(4):1067-77. doi: 10.1016/j.neuron.2015.04.014. PubMed Central PMCID:
871 PMC5077164.
- 872 49. Bakhurin KI, Goudar V, Shobe JL, Claar LD, Buonomano DV, Masmanidis SC. Differential
873 Encoding of Time by Prefrontal and Striatal Network Dynamics. *The Journal of Neuroscience*.
874 2017;37(4):854-70. doi: 10.1523/jneurosci.1789-16.2017. PubMed PMID: 28123021; PubMed
875 Central PMCID: PMC5296780.
- 876 50. Stokes MG, Kusunoki M, Sigala N, Nili H, Gaffan D, Duncan J. Dynamic Coding for Cognitive
877 Control in Prefrontal Cortex. *Neuron*. 2013;78(2):364-75. doi: 10.1016/j.neuron.2013.01.039.
878 PubMed PMID: 23562541; PubMed Central PMCID: PMC3898895.
- 879 51. MacDonald Christopher J, Lepage Kyle Q, Eden Uri T, Eichenbaum H. Hippocampal “Time Cells”
880 Bridge the Gap in Memory for Discontiguous Events. *Neuron*. 2011;71(4):737-49. doi:
881 <http://dx.doi.org/10.1016/j.neuron.2011.07.012>.
- 882 52. Cone I, Shouval HZ. Learning precise spatiotemporal sequences via biophysically realistic learning
883 rules in a modular, spiking network. *eLife*. 2021;10:e63751. doi: 10.7554/eLife.63751.
- 884 53. Maes A, Barahona M, Clopath C. Learning spatiotemporal signals using a recurrent spiking network
885 that discretizes time. *PLOS Computational Biology*. 2020;16(1):e1007606. doi:
886 10.1371/journal.pcbi.1007606.
- 887 54. Hardy NF, Buonomano DV. Encoding Time in Feedforward Trajectories of a Recurrent Neural
888 Network Model. *Neural Comput*. 2018;30(2):378-96. doi: 10.1162/neco_a_01041. PubMed PMID:
889 29162002; PubMed Central PMCID: PMC5873300.
- 890 55. Tupikov Y, Jin DZ. Addition of new neurons and the emergence of a local neural circuit for precise
891 timing. *PLOS Computational Biology*. 2021;17(3):e1008824. doi: 10.1371/journal.pcbi.1008824.
- 892 56. Gámez J, Mendoza G, Prado L, Betancourt A, Merchant H. The amplitude in periodic neural state
893 trajectories underlies the tempo of rhythmic tapping. *PLOS Biology*. 2019;17(4):e3000054. doi:
894 10.1371/journal.pbio.3000054.

- 895 57. Merchant H, Pérez O, Bartolo R, Méndez JC, Mendoza G, Gámez J, et al. Sensorimotor neural
896 dynamics during isochronous tapping in the medial premotor cortex of the macaque. *European*
897 *Journal of Neuroscience*. 2015;41(5):586-602. doi: <https://doi.org/10.1111/ejn.12811>.
- 898 58. Taxidis J, Pnevmatikakis EA, Dorian CC, Mylavarapu AL, Arora JS, Samadian KD, et al.
899 Differential Emergence and Stability of Sensory and Temporal Representations in Context-Specific
900 Hippocampal Sequences. *Neuron*. 2020. doi: 10.1016/j.neuron.2020.08.028.
- 901 59. Murakami M, Vicente MI, Costa GM, Mainen ZF. Neural antecedents of self-initiated actions in
902 secondary motor cortex. *Nat Neurosci*. 2014;17(11):1574-82. doi: 10.1038/nn.3826
- 903 60. Jin DZ, Fujii N, Graybiel AM. Neural representation of time in cortico-basal ganglia circuits. *Proc*
904 *Natl Acad Sci U S A*. 2009;106(45):19156-61. doi: 10.1073/pnas.0909881106. PubMed PMID:
905 19850874; PubMed Central PMCID: PMC2776432.
- 906 61. Mendoza G, Méndez JC, Pérez O, Prado L, Merchant H. Neural basis for categorical boundaries in
907 the primate pre-SMA during relative categorization of time intervals. *Nature Communications*.
908 2018;9(1):1098. doi: 10.1038/s41467-018-03482-8. PubMed PMID: 29545587; PubMed Central
909 PMCID: PMC5854627.
- 910 62. Duysens J, Schaafsma SJ, Orban GA. Cortical Off Response Tuning for Stimulus Duration. *Vision*
911 *Res*. 1996;36(20):3243-51. doi: [http://dx.doi.org/10.1016/0042-6989\(96\)00040-5](http://dx.doi.org/10.1016/0042-6989(96)00040-5).
- 912 63. Chubykin AA, Roach EB, Bear MF, Shuler MGH. A Cholinergic Mechanism for Reward Timing
913 within Primary Visual Cortex. *Neuron*. 2013;77(4):723-35. PubMed PMID: 23439124; PubMed
914 Central PMCID: PMC3597441.
- 915 64. Merchant H, Pérez O, Zarco W, Gámez J. Interval Tuning in the Primate Medial Premotor Cortex as
916 a General Timing Mechanism. *The Journal of Neuroscience*. 2013;33(21):9082-96. doi:
917 10.1523/jneurosci.5513-12.2013.
- 918 65. Buonomano DV, Maass W. State-dependent Computations: Spatiotemporal Processing in Cortical
919 Networks. *Nat Rev Neurosci*. 2009;10:113-25. doi: 10.1038/nrn2558. PubMed PMID: 19145235;
920 PubMed Central PMCID: PMC2676350.
- 921 66. Rigotti M, Barak O, Warden MR, Wang X-J, Daw ND, Miller EK, et al. The importance of mixed
922 selectivity in complex cognitive tasks. *Nature*. 2013;497(7451):585-90. doi: 10.1038/nature12160
- 923 67. DePasquale B, Cueva CJ, Rajan K, Escola GS, Abbott LF. full-FORCE: A target-based method for
924 training recurrent networks. *PLOS ONE*. 2018;13(2):e0191527. doi: 10.1371/journal.pone.0191527.
- 925 68. Murray JM, Escola GS. Learning multiple variable-speed sequences in striatum via cortical tutoring.
926 *eLife*. 2017;6:e26084. doi: 10.7554/eLife.26084.
- 927 69. Jazayeri M, Afraz A. Navigating the Neural Space in Search of the Neural Code. *Neuron*.
928 2017;93(5):1003-14. doi: <http://dx.doi.org/10.1016/j.neuron.2017.02.019>.
- 929 70. Laje R, Buonomano DV. Robust timing and motor patterns by taming chaos in recurrent neural
930 networks. *Nat Neurosci*. 2013;16(7):925-33. doi: 10.1038/nn.3405. PubMed PMID: 23708144;
931 PubMed Central PMCID: PMC3753043.
- 932 71. Monteforte M, Wolf F. Dynamic Flux Tubes Form Reservoirs of Stability in Neuronal Circuits.
933 *Physical Review X*. 2012;2(4):041007.
- 934 72. Chaisangmongkon W, Swaminathan SK, Freedman DJ, Wang XJ. Computing by Robust
935 Transience: How the Fronto-Parietal Network Performs Sequential, Category-Based Decisions.
936 *Neuron*. 2017;93(6):1504-17 e4. doi: 10.1016/j.neuron.2017.03.002. PubMed PMID: 28334612;
937 PubMed Central PMCID: PMC5586485.
- 938 73. Rabinovich MI, Simmons AN, Varona P. Dynamical bridge between brain and mind. *Trends Cogn*
939 *Sci*. 2015;19(8):453-61. Epub 2015/07/08. doi: 10.1016/j.tics.2015.06.005. PubMed PMID:
940 26149511.
- 941 74. Afraimovich V, Zhigulin V, Rabinovich M. On the origin of reproducible sequential activity in
942 neural circuits. *Chaos: An Interdisciplinary Journal of Nonlinear Science*. 2004;14:1123-9.
- 943 75. Rajan K, Abbott LF, Sompolinsky H. Stimulus-dependent suppression of chaos in recurrent neural
944 networks. *Physical Rev E*. 2010;82:011903(5).

- 945 76. Vogels TP, Rajan K, Abbott LF. Neural network dynamics. *Annu Rev Neurosci.* 2005;28:357-76.
946 PubMed PMID: 16022600.
- 947 77. Kim R, Sejnowski TJ. Strong inhibitory signaling underlies stable temporal dynamics and working
948 memory in spiking neural networks. *Nature Neuroscience.* 2021;24(1):129-39. doi: 10.1038/s41593-
949 020-00753-w.
- 950 78. Kim R, Li Y, Sejnowski TJ. Simple framework for constructing functional spiking recurrent neural
951 networks. *Proc Natl Acad Sci U S A.* 2019;116(45):22811-20. doi: 10.1073/pnas.1905926116.
952 PubMed PMID: 31636215; PubMed Central PMCID: PMC6842655.
- 953 79. Song HF, Yang GR, Wang XJ. Training Excitatory-Inhibitory Recurrent Neural Networks for
954 Cognitive Tasks: A Simple and Flexible Framework. *PLoS Comput Biol.* 2016;12(2):e1004792. doi:
955 10.1371/journal.pcbi.1004792. PubMed PMID: 26928718; PubMed Central PMCID:
956 PMC684771709.

957

958

Supporting information:

960 **S1 Fig. Generalization difference between the 2-Context and 2-Stimulus tasks are robust across different input**
 961 **parameters.** (A) Training on the 2-Context task with different analog context level pairs to signal the short (blue) and
 962 long (green) intervals (top), produced similarly timed short (blue) and long (green) intervals (bottom). Dashed lines
 963 denote the threshold used to measure the crossing time. (B) Training on 2-Stimulus task across different levels of
 964 overlap between the two input weight vectors (overlap ratio), quantified by the angle between the two weight vectors
 965 (top), and the corresponding learned output traces for short (blue) and long (green) intervals (bottom). (C) The mean
 966 (top) and standard deviations (bottom) of the crossing times across 10 simulations for the generalization experiments
 967 corresponding to the five conditions as in (A). (D) same as (C) but for 2-Stimulus task. (E) The sigmoid fit slopes of
 968 the generalization experiments in the five conditions of 2-Context task (cyan, as in A) were significantly lower than
 969 that for 2-Stimulus task (orange, as in B): two-way ANOVA, $F_{1,90} = 123.1$, $P < 0.0001$ (Left). The absolute correlation
 970 coefficients of the generalization experiments in the five conditions for 2-Context task (cyan, as in A) were
 971 significantly higher than that of the 2-Stimulus task (orange, as in B): two-way ANOVA on the Fisher-transformed
 972 data, $F_{1,90} = 374.2$, $P < 0.0001$ (right). (F) The mean error across all tested levels of the noise perturbation experiments
 973 in the five conditions for 2-Context task (cyan, as in A) is significantly higher than that for 2-Stimulus task (orange,
 974 as in B): two-way ANOVA, $F_{1,90} = 106.1$, $P < 0.0001$ (Left). Right, the same as the left but for standard deviations of
 975 the crossing times: two-way ANOVA, $F_{1,90} = 625.7$, $P < 0.0001$.

976
 977 **S2 Fig. Superior generalization in the RNNs trained on the 2-Context task is maintained in the absence of a Go**
 978 **stimulus** (A) Schematic of the 2-Context task without the Go stimulus. (B) Left, the sigmoid fit slopes in the
 979 generalization experiments for the 2-Context task without Go stimulus are not significantly different from the original
 980 2-Context task, and still significantly lower than that for the standard 2-Stimulus task (one-way ANOVA with posthoc
 981 Tukey test, $F_{2,27} = 53.4$, ns: $P = 0.669$, ****: $P < 0.0001$). Right, the absolute correlation coefficients in the
 982 generalization experiments for the 2-Context task without Go stimulus not significantly different from the 2-Context
 983 task but significantly higher than that for the standard 2-Stimulus task (one-way ANOVA on the Fisher-transformed
 984 data with posthoc Tukey test, $F_{2,27} = 112.9$, ns: $P = 0.957$, ****: $P < 0.0001$).

985
 986 **S3 Fig. Generalization in the 2-Context task relies on continuous input.** (A) Schematic of the standard 2-Context
 987 task with persistent context input. (B) Schematic of a task in which the two intervals are signaled by the same brief
 988 input, but with different analog values. (C) Plots of the mean crossing time for each RNN across input conditions for
 989 the persistent (top) and transient (bottom) tasks. (D) Left, mean slope of the sigmoid fits for transient input task is
 990 significantly higher than that for the persistent 2-Context task ($n = 10$ simulations for each, two-sided t test, $t_{18} = 9.98$,
 991 $P < 0.0001$). Right, correlation coefficient between mean crossing times and input conditions for transient 2-Context
 992 is significantly lower than that for the persistent 2-Context task ($n = 10$ simulations for each, two-sided t test on Fisher-
 993 transformed values, $t_{18} = 7.52$, $P < 0.0001$). (E) Standard deviations of the crossing times for each RNN in the
 994 persistent 2-Context (top) and transient 2-Context (bottom) tasks, as a function of input conditions.

995
 996 **S4 Fig. Changing the initial gain of the recurrent weight matrix to 1.5 does not alter the generalization and**
 997 **robustness to noise differences between the 2-Context and 2-Stimulus tasks.** (A) Plots of the mean crossing time
 998 for each RNN across input conditions for the 2-Context (top) and 2-Stimulus (bottom) tasks. Insets, examples of the
 999 sigmoid-function fits for a single RNN (black). (B) Left, mean slope of the sigmoid fits for 2-Stimulus task is
 1000 significantly higher than that for the 2-Context task ($n = 20$ simulations for each, two-sided t test, $t_{18} = 6.91$, $P <$
 1001 0.0001). Right, correlation coefficient between mean crossing times and input conditions for 2-Context task is
 1002 significantly higher than that for the 2-Stimulus task ($n = 20$ simulations for each, two-sided t test on Fisher-
 1003 transformed values, $t_{18} = 16.56$, $P < 0.0001$). (C) Standard deviations of the crossing times for each RNN in the 2-
 1004 Context (top) and 2-Stimulus (bottom) tasks, as a function of input conditions. (D) Left, mean error (across 50 trials)
 1005 for 2-Context task (cyan) is higher than that for 2-Stimulus task (orange) ($n = 10$ simulations, two-way ANOVA with
 1006 mixed-effect design, $F_{1,18} = 32.48$, $P < 0.0001$). Right, mean standard deviation of the time of threshold-crossing
 1007 across all correct trials for 2-Context task (cyan) is higher than that for 2-Stimulus task (orange) ($F_{1,18} = 128.50$, $P <$
 1008 0.0001). Data are presented as mean \pm SEM.

1009

1010 **S5 Fig. Full initial connectivity of the weight matrix does not alter the generalization and robustness to noise**
1011 **differences between the 2-Context and 2-Stimulus tasks.** (A) Plots of the mean crossing time for each RNN across
1012 input conditions for the 2-Context (top) and 2-Stimulus (bottom) tasks. Insets, examples of the sigmoid-function fits
1013 for a single RNN (black). (B) **Left**, mean slope of the sigmoid fits for 2-Stimulus task is significantly higher than that
1014 for the 2-Context task ($n = 20$ simulations for each, two-sided t test, $t_{18} = 4.35$, $P = 0.00039$). **Right**, correlation
1015 coefficient between mean crossing times and input conditions for 2-Context task is significantly higher than that for
1016 the 2-Stimulus task ($n = 20$ simulations for each, two-sided t test on Fisher-transformed values, $t_{18} = 6.48$, $P < 0.0001$).
1017 (C) Standard deviations of the crossing times for each RNN in the 2-Context (top) and 2-Stimulus (bottom) tasks, as
1018 a function of input conditions. (D) **Left**, mean error (across 50 trials) for 2-Context task (cyan) is higher than that for
1019 2-Stimulus task (orange) ($n = 10$ simulations, two-way ANOVA with mixed-effect design, $F_{1,18} = 5.78$, $P = 0.027$).
1020 **Right**, mean standard deviation of the time of threshold-crossing across all correct trials for 2-Context task (cyan) is
1021 higher than that for 2-Stimulus task (orange) ($F_{1,18} = 86.03$, $P < 0.0001$). Data are presented as mean \pm SEM.
1022

1023 **S6 Fig. Differential functional effects of deleting specific classes of units.** (A) Schematic of the deletion
1024 experiments. To delete a given unit denoted by the red arrow (bottom), all in and out weights of the recurrent weight
1025 matrix of that unit were set to zero. (B) Performance of RNNs trained on the 2-Context task after progressively
1026 deleting units from specific temporal classes: stimulus-specific, scaling, and absolute temporal classes for both
1027 excitatory (left) and inhibitory (right) units. For each data point, units were randomly selected 10 times, and 10 test
1028 trials were obtained. A three-way ANOVA revealed highly significant effects of main temporal-class ($F_{2,619} = 31$, $P <$
1029 10^{-12}) and Ex-Inh ($F_{2,619} = 390$, $P < 10^{-66}$) factors. Additionally, there was a highly significant interaction between
1030 temporal-class and Ex-Inh class ($F_{2,619} = 27$, $P < 10^{-10}$) and multi-comparison analyses showed that performance for
1031 inhibitory scaling cells was significantly lower than all other 5 deletion manipulations ($P < 0.0001$ for all comparisons).
1032 (C) Similar to (B) but for error. As in (B), there were highly significant main effects ($F_{2,619} = 34$, $P < 10^{-14}$, and $F_{2,619}$
1033 $= 118$, $P < 10^{-24}$, for temporal-class and Ex-Inh, respectively), as well as a significant interaction between temporal-
1034 class and Ex-Inh ($F_{2,619} = 46$, $P < 10^{-18}$). And again the inhibitory scaling cells increased the error more than all other
1035 deletion manipulations ($P < 0.0001$ for all comparisons). (D-E) There were no main effects of temporal-class or Ex-
1036 Inh that were consistently significant for both the performance and error measure. The interaction between temporal-
1037 class and Ex-Inh was either trending ($F_{2,619} = 2.5$, $P = 0.08$) or mildly significant ($F_{2,619} = 3.6$, $P = 0.027$) for the
1038 performance and error analyses, respectively. Data are presented as performance mean \pm SEM across 20 RNNs. Notice
1039 that the performance of stimulus-specific units in (D) and (E) (magenta) are very similar to, and mostly obscured by
1040 the absolute traces (red). (F) Mean output traces across 20 simulations when deleting 6 excitatory (left) and inhibitory
1041 (right) units of the three types: stimulus-specific, scaling, and absolute for 2-Context task. (G) Same as F but for 2-
1042 Stimulus task.
1043

1044 **S7 Fig. Differential subspace dynamics for RNNs trained on 2-Context and 2-Stimulus tasks.** (A) For the 2-
1045 Context task, recurrent unit dynamics for the short (blue) and long (green) intervals were projected into the first three
1046 PC spaces. Asterisks denote the onset of inputs ($t=0$), arrows denote the corresponding weights vectors (Input_{Go}, black;
1047 Input_{Context}, cyan; and Output, red) projected onto the same PC space. Color dots denote the 250 ms intervals along
1048 each trajectory. Inset, schematic of angles between segments of the approximate RNN trajectory (orange) and the
1049 three weight vectors. These vectors were used to compute the pairwise angles to the Input_{Go}, Input_{Context} and Output
1050 vectors. (B) Similar to (A) but for 2-Stimulus task, but here the two input vectors represented the Input_{Short} (blue) and
1051 Input_{Long} (green) weight vectors. (C) Same number of PCs explained more variance for 2-Context task than that for 2-
1052 Stimulus task (Two-way ANOVA, $F_{(1,38)} = 255.6$ and $P < 0.0001$). (D) Average pairwise angles between segments of
1053 short (top)/long (bottom) dynamics and inputs/output vectors as in (A) for 2-Context task (20 simulations, data
1054 presents as Mean \pm SEM). Shaded area denoted the duration of the transient Input_{Go} (E) Same as in (D) but for 2-
1055 Stimulus task. The shaded area denotes the duration of the transient Input_{Short} and Input_{Long}.
1056
1057

1058 **S8 Fig. PCA plots of the recurrent dynamics for generalization to novel intervals** (A) Recurrent dynamics
1059 corresponding to different context levels (denoted by the color) as in Fig. 2 were projected into the first three PCs in
1060 20 RNNs trained on 2-Context task. The arrows denoted the directions of Input_{Go} (black), Input_{Context} (cyan), and
1061 Output (red) weights projected into the same PC space. (B) similar as in (A) but for the 2-Stimulus task.
1062

1063 **Author contributions:**

1064 Conceptualization: SZ, DVB, SCM
1065 Formal analysis: SZ, DVB
1066 Methodology: SZ, DVB
1067 Supervision: SCM, DVB
1068 Visualization: SZ
1069 Funding acquisitions: SCM, DVB
1070 Writing—original draft: SZ, DVB, SCM
1071 Writing—review & editing: SZ, DVB

1072

1073

1074 **Data and codes availability**

1075 All data are available in the main text or supplementary materials. Codes used for the simulations
1076 in this paper are available at (https://github.com/ShanglinZhou/RNN_2Intervals).

1077

1078

1079